

General Disclaimer

One or more of the Following Statements may affect this Document

- This document has been reproduced from the best copy furnished by the organizational source. It is being released in the interest of making available as much information as possible.
- This document may contain data, which exceeds the sheet parameters. It was furnished in this condition by the organizational source and is the best copy available.
- This document may contain tone-on-tone or color graphs, charts and/or pictures, which have been reproduced in black and white.
- This document is paginated as submitted by the original source.
- Portions of this document are not fully legible due to the historical nature of some of the material. However, it is the best reproduction available from the original submission.

NASA CONTRACTOR REPORT

The Interaction of Small Metal Particles with Refractory
Oxide Supports

Ch. Park
K. Heinemann

(NASA-CR-176228) THE INTERACTION OF SMALL
METAL PARTICLES WITH REFRACTORY OXIDE
SUPPORTS Final Technical Report (Eloret
Corp.) 85 p HC A05/MF A01 CSCL 20L

N86-11047

Unclas

G3/76 15218

CONTRACT NAS2-
NCC2-248
March 4, 1985

NASA

NASA CONTRACTOR REPORT

The Interaction of Small Metal Particles with Refractory
Oxide Supports

Ch. Park
K. Heinemann

Eloret Institute
1178 Maraschino Drive
Sunnyvale, CA 94087

Prepared for
NASA Ames Research Center
under Grant NCC2-248



National Aeronautics and
Space Administration

Ames Research Center
Moffett Field, California 94035



1. Report No.	2. Government Accession No.	3. Recipient's Catalog No.	
4. Title and Subtitle THE INTERACTION OF SMALL METAL PARTICLES WITH REFRACTORY OXIDE SUPPORTS		5. Report Date 4 March, 1985	6. Performing Organization Code
		8. Performing Organization Report No.	
7. Author(s) Ch. Park and Klaus Heinemann		10. Work Unit No.	
9. Performing Organization Name and Address Eloret Institute 1178 Maraschino Drive Sunnyvale, CA 94087		11. Contract or Grant No. NCC2-248	
		13. Type of Report and Period Covered Final Technical Rep.	
12. Sponsoring Agency Name and Address NASA Ames Research Center Moffett Field, CA 94035		14. Sponsoring Agency Code 503-56-11	
		15. Supplementary Notes Contact Person: Dr. H. Poppa, Technical Monitor NASA Ames Research Center, (415) 694-6141	
16. Abstract Islands and continuous layers of Pd were grown in UHV on Mo and MoO substrates. As-deposited Pd islands and layers exhibited bulk Pd adsorption properties for CO when the Pd had been deposited at RT and at thicknesses exceeding 3 ML. However, CO adsorption was drastically reduced upon annealing. This deactivation was interpreted in terms of substrate/support interaction involving the diffusion of substrate species toward the Pd surface, using AES, TPD, and work function measurement techniques. A study of the growth and annealing behavior of Pd on Mo(110) was made for thicknesses up to 12 monolayers and substrate temperatures up to 1300K, using AES, XPS, LEED, and work function measurements. At low temperatures Pd formed a monolayer without alloying. In thick layers (12 ML) annealed above 700 K, Mo diffusion into the Pd layer and alloying were noted. Such layers remained continuous up to 1100 K. Thinner Pd layers were less stable and started coalescing upon annealing to as little as 550 K. Significant changes in Pd Auger peak shape, as well as shifts of Pd core levels, were observed during layer growth and annealing.			
17. Key Words (Suggested by Author(s)) Metal/Support Interaction CO Decomposition Small Particles/clusters NiCrAl - S Surface segregation		18. Distribution Statement Unclassified - Unlimited Subject category 076	
19. Security Classif. (of this report) Unclassified	20. Security Classif. (of this page) Unclassified	21. No. of Pages	22. Price*

THE INTERACTION OF SMALL METAL PARTICLES WITH

REFRACTORY OXIDE SUPPORTS

Final Technical Report
for the period
May 20, 1983 - October 31, 1984

Submitted to

National Aeronautics and Space Administration
Ames Research Center
Moffett Field, CA 94305

Computation Chemistry and Aerothermodynamics Branch
Dr. Jim Arnold, Chief
Dr. Helmut Poppa, Technical Monitor

NASA-Grant No. 1
NCC 2-248

Prepared by

ELORET INSTITUTE
1178 Maraschino Drive
Sunnyvale, CA 94087
(Phone: (408) 730-8422)
K. Heinemann, President and Co-Principal Investigator
Chan Park, Principal Investigator

THE INTERACTION OF SMALL METAL PARTICLES WITH REFRACTORY OXIDE SUPPORTS

Islands and continuous layers of Pd were grown in ultra-high vacuum on molybdenum oxide and clean molybdenum substrates. The oxide layer was prepared by heating a Mo(110) crystal at 1250 K in 5×10^{-8} mbar of oxygen for 7 minutes and was characterized by LEED to have a stable $c(14 \times 7)$ structure. The Auger peak to peak ratio of O/Mo was 0.25. The clean Mo substrates were (110)-oriented. The Pd depositions were performed from a wire sublimation source at rates of approximately 0.1 monolayers per minute while the background pressure remained below 3×10^{-10} mbar. Research-grade CO was adsorbed at saturation dosages of 6L. It was found that as-deposited Pd islands and layers exhibited bulk Pd adsorption properties for CO when the palladium had been deposited at RT at thicknesses in excess of about 3ML. CO adsorption was, however, drastically reduced upon annealing. For islands, annealing temperatures of as low as 400K led to some reduction in CO adsorption, whereas more severe reductions were found to occur at 600K for islands and at 800K for continuous multilayers. The deactivation depended on the Pd thickness, the substrate species, and the extent of thermal treatments. Auger electron spectroscopy (AES), thermal programmed desorption (TPD), and work function measurements were combined to interpret the deactivation behavior in terms of substrate/support interactions involving the diffusion of substrate species towards the Pd surface. A full report of this work (1) is included as Appendix 1.

The growth and annealing behavior of Pd on Mo(110) was studied in more detail for the deposit thicknesses up to 12 monolayers and substrate temperatures up to 1300K, using AES, XPS, LEED, and work function change measurements. Similar to earlier work done on Pd/W(110) by W. Schlenk and E. Bauer (Surf. Sci. 93, 1980, 9), Pd was found to form a monolayer without alloying, but the LEED structure in the submonolayer range is different from Pd/W(110) after heating to 700K. In thick layers (12 ML) annealed above 700K, clear evidence of Mo diffusion into the Pd layer and alloying have been seen. Such layers remained continuous up to 1100K. Thinner Pd layers were found less stable and start coalescing into 3-dimensional crystallites upon annealing between 550 and 650 K; above 770 K they form Pd/Mo alloy islands covered by a Pd monolayer and surrounded by a Pd monolayer-covered alloy monolayer. Significant changes in Pd Auger peak shape, as well as shifts of Pd core levels, are observed during layer growth and annealing. A detailed report on this work (2) is included as Appendix 2.

Other work performed in part under support of NASA-Grant NCC2-248 includes:

(1) CO Desorption from Supported Ru Particles (3).

The low-pressure interaction of CO with small Ru particles supported on UHV-cleaved muscovite mica has been studied, using flash thermal desorption, AES, transmission electron microscopy (TEM) and transmission electron diffraction (TED) techniques. Average particle

sizes ranged from 1.2 to 6 nm. No evidence of CO decomposition on Ru was found over pressure and temperature ranges from 10^{-11} to 10^{-6} mbar and 570 - 800 K, respectively. Gas and temperature treatments did, however, cause significant particle size dependent changes in the morphology and dispersion of the Ru particles, which in turn affected the CO desorption.

(ii) Surface Segregation of Minor Constituents in NiCrAl using AES and XPS (4).

After heating to 1100K in UHV, the surface segregation of minor constituents in undoped and Zr and Y-doped NiCrAl alloys shows considerable differences. In the undoped alloy, the surface becomes rich in sulphur, whereas in Zr and Y doped alloys the segregation of S to the surface is suppressed. Comparison of AES and XPS results suggests that Zr is more effective than Y in the suppression of S surface segregation. Preliminary results from in-situ oxidation of the alloys strongly supports the view that Zr not only inhibits the segregation of S, a possible cause of oxide spalling, but also modifies the rate of formation of an Al₂O₃ layer.

(iii) The Role of some Minor Constituents in NiCrAl Superalloys: The Effect of a Surface Layer of Zr on the Segregation of Sulphur (5).

In order to separate bulk and surface effects of the inhibition by Zr doping of S surface segregation upon heating of NiCrAl alloys in UHV, several monolayers of Zr were evaporated onto undoped NiCrAl and annealed up to 1000 K. Sulphur still readily segregated, showing that the apparent competition for segregation to the surface is not a

**ORIGINAL PAGE IS
OF POOR QUALITY**

free-surface effect, but a consequence of the NiCrAlZr bulk matrix.

The following papers, referenced in the preceding summary report and resulting from work supported under NASA-Grant NCC2-248, were prepared for publication in scientific journals:

(1) "Metal Support Interactions (MSI) During the Adsorption of CO on Thin Layers and Islands of Epitaxial Pd," by Ch. Park, F. Soria, and H. Poppa, submitted for publication. (Preprint included as Appendix 1).

(2) "Growth and Alloying of Pd Films on Mo(110) Surfaces," by Ch. Park, E. Bauer, and H. Poppa, submitted for publication. (Preprint included as Appendix 2; this paper was presented at the Annual Meeting of the American Vacuum Society in Reno, December 1984).

(3) "CO Desorption from Supported Ru Particles," by Ch. Park, W.G. Durrer, H. Poppa, and J.T. Dickinson, *J. Catalysis*, to be published.

(4) "Surface Segregation of Minor Constituents in NiCrAl Using AES and XPS," by F.A. Marks, Ch. Park, R. Browning, and J.L. Smialek, to be submitted for publication.

(5) "The Role of Some Minor Constituents in NiCrAl Superalloys: The

Effect of a Surface Layer of Zirconium on the Segregation of Sulphur," by R Browning, Ch. Park, F.A. Marks, and Ch. Papageorgopoulos, to be submitted for publication.

APPENDIX 1

METAL SUPPORT INTERACTIONS (MSI) DURING THE ADSORPTION OF CO ON THIN LAYERS AND ISLANDS OF EPITAXIAL PD

BY

Chan Park, Federico Soria and Helmut Poppa

Stanford/NASA Joint Institute for Surface and Microstructure Research

NASA Ames Research Center

Moffett Field, CA 94035

Summary

Islands and continuous layers of Pd were grown in UHV on substrates of Mo (110) c (14x7)-0, designated as MoO_x, and on clean Mo(110), respectively. It was found that as-deposited islands and layers exhibited bulk Pd adsorption properties for CO when deposited at RT and for Pd thicknesses in excess of about 3ML. CO adsorption was drastically reduced, however, upon annealing. For islands, annealing temperatures of as low as 400k led to some reduction in CO adsorption whereas more severe reductions were found to occur at 600k for islands and at 800k for continuous multilayers. The deactivation depended upon Pd thickness, substrate species, and on the extent of thermal treatments. AES, TPD, and $\Delta\phi$ measurements were combined to interpret the deactivation behavior in terms of substrate/support interactions involving the diffusion of substrate species towards the Pd surface.

Introduction

It has long been recognized that the physical and chemical properties of the material used as support for small metal particles and clusters can influence the catalytic properties of such a metal/support system to a significant degree. The first deliberate attempts to modify and direct the catalytic behavior of metal/support systems through

systematic control of metal/support interactions (MSI) date back to the work of Schwab⁽¹⁾ and Solymosi². Recently strong metal support interactions (SMSI) have received particular attention through the work of Tauster et.al.³, Vannice and coworkers⁽⁴⁾, and through a symposium⁵ focusing on this area of intensive current research, in which G. C. Bond⁶ pointed out the principal difficulty that is often encountered: distinguishing between intrinsic particle size effects, electronic interactions between metal and support, and other interactions such as poisoning of the metal by support contaminants and alloying. Furthermore, depending on the support material, interactions were classified into weak (e.g. Al_2O_3 , SiO_2), medium (zeolites), and strong (e.g. TiO_2) interactions, the latter ones featuring particularly drastic effects of high reducing temperatures during catalyst preparation upon CO and H_2 adsorption and upon catalytic reaction selectivities.

At first glance a very different kind of metal-support interaction has recently been discovered in thin metal overlayers on single crystal metal substrates. Overlayers of Pd in the monolayer thickness range on Nb(110) have been found⁷ not to adsorb H_2 and on W(110)⁸ not to adsorb CO, and we have previously published preliminary results⁹ on the drastic reduction of the adsorption of CO and H_2 on multilayer thick Pd films on Mo(110). It seems that here also the situation is comparable to the standard oxide support case in that genuine electronic¹⁰ vs. alloying or contamination effects have to be distinguished with great care.

Thick Pd films evaporated in UHV (often onto mica or Al_2O_3 substrates) and characterized by various surface analytical techniques have been used for model chemisorption studies in a number of cases¹¹⁻¹³

because of the relative ease of deposition of Pd by sublimation and because of the catalytic importance of this metal. Because of the different method of preparing continuous epitaxial Pd surfaces of varying orientation and differing degrees of cleanliness and microstructural morphology, results of gas adsorptions on deposited Pd films have sometimes been found to be very different^{13,9} from the respective results on bulk Pd surfaces prepared by repetitive heating and sputtering cycles¹⁴⁻¹⁹. However, more unambiguous experimental evidence needs to be accumulated before the influence of surface contaminants, micromorphology, and defect structure upon the adsorption of various active gases is clearly established²⁰⁻²²; carbon contamination being a particularly difficult experimental problem for Pd because of the overlap of the respective Auger peaks.

Very thin and well-defined particulate Pd deposits on mica and such refractory oxide substrates as Al_2O_3 and MgO have been used in UHV for catalytic model studies in this laboratory for a number of years²³⁻²⁶. Temperature programmed desorption of chemisorbed gases, ex- and in-situ transmission electron microscopy (TEM), and steady state low pressure gas reaction studies were combined in different variations of an integrated experimental approach²⁷, where the size of Pd particles was reproducibly varied between several hundred to less than 10\AA .

The growth of evaporated Pd layers on clean⁹ and oxidized Mo(110) substrates²⁸⁻²⁹ provides an opportunity to perform controlled gas adsorptions and desorptions simultaneously on both continuous Pd layers and on discontinuous flat islands and with increased precision for temperature, AES, and Pd flux control. In addition LEED and work

function measurements become possible and can be used to help interpret some of the unexpected previous results which concerned mainly a drastic reduction of CO and H₂ adsorption upon relatively mild annealing of island^{28,29} and continuous film⁹ deposits of larger than monolayer thickness. The present study was initiated after some experimental inconsistencies became apparent with further work. This has led to a reassessment of the originally used CO dosages and provided much additional information on the nature of the Pd surface deactivation process for CO adsorption by making intensive use of improved work function change ($\Delta\phi$) measurements. We will show that the high energy adsorption sites for CO on both islands and continuous multilayers of Pd can be preferentially deactivated by a thermally activated process probably involving substrate species. We also present evidence that strong electronic support interactions that affect CO adsorption are only important for Pd overlayers thinner than approximately 3 monolayers for this substrate support system. In a future report the present speculations about the specific nature of this substrate/overgrowth interaction process will be examined further.

Experimental

As described previously^{9,29}, the experiments were carried out in a standard UHV surface analysis chamber with facilities for LEED, for line of sight temperature programmed desorption (TPD, $\frac{\Delta T}{\Delta t} = 4\text{k/s}$) into a quadrupole mass spectrometer or by Kelvin probe work function measurements, for derivative AES, and for high temperature resistive heating of a single crystal Mo ribbon of (110) orientation. When needed a thermally stable 2-dimensional oxide layer characterized by a c(14x7)

LEED structure³⁰ was prepared by heating the Mo(110) crystal at 1250k in 5×10^{-8} Torr of O_2 for 7 min. resulting in an Auger peak to peak ratio of $O/Mo = .25$ (Mo crystals with this stable oxide layer are in the following referred to as MoO_x substrates). Pd was deposited from a well outgassed wire sublimation source with a deposition rate of approximately .1 ML/min which was calibrated by monitoring the Pd and Mo Auger amplitudes (AA) during RT layer by layer growth of Pd on clean Mo(100)³¹ (see Fig. 1). The background pressure during the deposition of a few monolayers of Pd remained below 1×10^{-10} Torr and never exceeded 2×10^{-10} Torr during the long time deposition of thick layers. The C (272 eV) + Pd (279 eV) : Pd (330 eV) Auger ratio was always smaller than 0.18 (for a modulation voltage of 2 Vp-p); it was used as a measure of carbon cleanliness and is 10 to 50% lower than previously reported handbook values for bulk Pd.

All CO dosages used in this study were saturation dosages of 6L, based upon nude ionization gauge pressure measurements in the main vacuum chamber. Research-grade CO was introduced via a standard leak valve from a higher pressure gas manifold line which was regularly checked with respect to gas purity.

Results and Discussion(1) Pd islands on MoO_x

Depending on the substrate temperature T_s during Pd deposition and deposition time t (or amount Q of Pd measured in "equivalent monolayers" E.ML grown on clean Mo(110)), islands of varying average thickness and with an increasing substrate coverage Θ_{Pd} can be grown on MoO_x -c (14x7) substrates²⁹. As also shown previously, Auger measurements of $\text{AA}_{\text{Pd,Mo}}$ as a function of t or Q can determine the average island thickness (in number of monolayers, n) and Θ_{Pd} . Islands thicker than approximately 3ML and as thick as 8-10ML can be prepared in the as-deposited state at room temperature.

What is not obtainable from Auger measurements is the average lateral extension of individual islands, for which a true Pd surface area measurement is needed. The area A_{TPD} under the first temperature programmed desorption spectrum, TPD(1), of a saturation dose of CO adsorbed at RT (see Fig. 2a as an example) can provide such a measurement. Table 1 list the Θ_{Pd} and A_{TPD} surface areas normalized to the case of $Q=10$ E.ML when practically total substrate surface coverage by Pd is obtained. As can be seen from Table 1, the A_{TPD} values do not differ significantly from Θ_{Pd} , an indication that the total surface areas of the islands are not much larger than their projected surface areas; or that the ratio (l/d) of lateral to "vertical" island dimension is quite large - even for the thin deposits where large surface area contributions from non-horizontal island surfaces could have been expected. (The l/d and l values also given in table 1 are based on the simplest possible model geometry of the islands, namely square boxes of "size" l and thickness d). It is clear,

therefore, that thin but rather large flat islands are growing at RT on this substrate, which is not too surprising since rather good "wetting" is expected in view of the only modestly reduced deposit/substrate interaction on this semi-oxide type substrate³².

If the shape rather than just the area of saturated (6L) CO thermal desorption curves from as-deposited Pd islands is considered (see all (1) curves in Fig. 2 for a selection of Pd coverages), it is obvious that different contributions from high and low-energy adsorption sites are present. The thinner deposits have a slightly higher proportion of low energy ¹⁹, or 2-fold¹⁵ sites (peak temperature $T_p \approx 380k$) when compared to the higher energy ₂¹⁹ or 3-fold¹⁵ sites ($T_p \approx 425k$). This is the same trend that was noticed quite unambiguously in our previous work with CO adsorption on small Pd particles grown on 2 different orientations of sapphire substrates^{25,27,33}. Since the high energy sites were more preferred on both large and better (111) oriented particles, and the contribution from low energy sites definitely increased with decreasing particle size (down to about 15 Å diameter), we tentatively correlated the high energy sites with adsorption on (111) facet planes of the particles and the low energy sites with lower coordination corner and edge sites.

If this argument holds also in the present situation we would have to assign the $T_p \approx 425k$ peak to desorption from the (111) oriented flat island tops. LEED results on high Pd coverage island films also showed good (111) perfection (1x1 pattern) so that a good epitaxial 2-degree orientation probably could also be inferred for the smaller island size deposits.

Annealing, however, changes the adsorption behavior of CO on these Pd island films drastically. One form of annealing is simply the heating that the deposit experiences during the first thermal desorption: TPD(1). As demonstrated in Fig. 2, the second TPD in all four cases leads to a desorption spectrum with sharply decreased peak areas and with the preferred elimination of high energy adsorption sites. (If TPD (2) is repeated only minor changes result). The search for what can cause such drastic changes with respect to the normal adsorption behavior of CO on bulk Pd¹⁴⁻¹⁹ will be the subject of much of the remaining discussions in the paper.

First of all a reduction of active metal area can occur during massive coalescence and concomitant 3-dimensional island growth. But for this to be happening the respective Pd Auger amplitudes (given in Fig. 2) and the substrate/overgrowth Auger amplitude ratios (Mo/Pd in Fig. 2) would have to change much more drastically than shown. These Auger data can be explained either by small island rearrangements or by the adsorption of as yet unidentified species migrating towards the island surfaces, or by a combination of these mechanisms. In both cases the Pd Auger emission would be reduced slightly and it is conceivable that surface "poisoning" would be accompanied by a strong reduction in CO adsorption on preferred sites.

More and better defined annealing studies were conducted to help elucidate the nature of the thermally activated island deactivation process. Fig. 3 shows 1st TPD spectra of 2 E.ML thick fresh deposits that were subjected to 2 min anneals at the indicated substrate

temperatures T_a before they were dosed with CO (6L at RT) for the subsequent thermal desorptions. The results prove that heat treatments at as low as 80K above RT affect the subsequent adsorption of CO in a clearly noticeable way, and preannealing temperatures above 600k cause a severe reduction of the adsorption capability of the Pd islands. As found previously, the high energy adsorption sites were preferentially eliminated, and the peak temperature for the remaining sites dropped to about 350k. It seems obvious, therefore, that even very mild heat treatments caused small rearrangements of Pd islands on MoO_x and/or deactivating substrate species such as O, Mo, or MoO_y easily diffused onto the originally clean Pd island surfaces.

The temperature regions which caused particularly severe changes in the surface properties of the Pd islands were indicated best by $\Delta\phi$ measurements. Fig. 4 shows an example of a 3 E.ML thick film that was subjected to successive 2 min anneals at increasing substrate temperatures which were followed by AA and $\Delta\phi$ measurements at RT inbetween anneals. The $\Delta\phi$ data clearly point out the temperature regions of 500-700K and 800-1000k that caused particularly strong changes, a result which is corroborated by TPD measurements after consecutive high T_a anneals (see Fig. 12 which represents a comparative summary of A_{TPD} results). It is surprising, however, to see in Fig. 3 how comparatively little the corresponding Auger measurements reflect the above mentioned surface property changes of the Pd islands; an indication that only relatively minor rearrangements of island shapes and dimensions occur up to 650k and that major changes take place only above 900k. But such changes are very sensitively detected by $\Delta\phi$ measurements.

Pd deposits of much higher substrate coverage, θ_{Pd} , and correspondingly greater average island thickness - see ref. (27) - were more useful for Auger measurements which were intended to pinpoint more clearly the diffusion of surface species during annealing. Fig. 5 shows the annealing behavior of a much thicker island film ($Q \approx 8$ E.M.L), and when compared to the 3 E.M.L thick film of Fig. 4 it is quite apparent that major changes in island "dispersion" only occur for $T_a \gtrsim 700k$ perhaps an indication of diffusion retarded by greater film thickness. Furthermore, the behavior of the AA for oxygen and Pd from 500-700k indicates some diffusion of substrate O into the Pd islands³⁴ in this temperature range. Above 700k either island shrinkage/thickening or surface precipitation of Mo or some MoO_y species - or a combination of both - can again be inferred from the Auger annealing data.

Further evidence for the role of thermally activated diffusion and/or island rearrangement processes in deactivating Pd island deposits is contributed by the effect of elevated substrate temperatures T_s maintained during Pd deposition. A T_s of only 500k during Pd growth ($t = 50$ min. for $Q=5$ E.M.L) leads to well ordered Pd island films with severely reduced adsorption capability for CO. The TPD spectrum consists only of a small low energy peak with $T_p = 360k$.

(2) Continuous Pd layers on Mo(110)

In the absence of other Auger detectable impurities, O and Mo substrate species were suspected of causing the above mentioned deactivation of Pd island surfaces, and some preliminary evidence for O deactivation was presented previously²⁹. However, it is obviously very difficult to distinguish by Auger between O on the substrate and O on the Pd islands. Therefore, CO adsorption studies on continuous Pd

layers, grown on clean Mo (110), were initiated. The other reason was the intention of directly correlating the adsorption behavior on thin films of Pd with adsorption data on bulk Pd single crystals as reported by many investigators in the past¹⁴⁻¹⁹. TPD measurements were also needed from thick, continuous Pd deposits to calibrate the mass spectrometer sensitivity for desorbing CO.

Auger amplitude measurements for the RT growth of Pd/Mo(110) were presented in Fig. 1. They proved the layer by layer growth mechanism during the early stage of deposition. In view of many previous results of metal layers growing on metallic substrates (see, for instance, the review by E. Bauer³⁵), which indicate that quasi-two-dimensional layers reach bulk metallic properties only after several layers have been deposited (usually $n \sim 5$) and that in the case of Pd/W(110)³⁶ particularly strong deviations of surface properties ($\Delta\phi$) were noted for $n < 3$, it first had to be established what "critical" thickness behavior pertained in the case of Pd/Mo(110). Furthermore, a report³⁷ on the anomalous adsorption of CO and O₂ on Pd layers less than 3 ML thick and our own CO adsorption results for Pd/MoO_x indicate that the "critical Pd layer thickness" to reach bulk adsorption also had to be established for Pd/Mo(110).

Bare metal work function ($\Delta\phi$) and CO adsorption/thermal desorption measurements in the critical layer thickness range are presented in Fig. 6a and 6b, respectively. The $\Delta\phi^{\text{Pd}}$ data are given for successive RT Pd dosages and for successive depositions at RT followed each time by a 2 min anneal at $T_a = 800\text{k}$. The results are quite similar to the case of Pd/W(110)³⁶ although we tend towards interpreting the 800k measurements more in terms of diffusional adsorption of substrate

species to the Pd surface rather than by massive coalescence and 3-dimensional growth of thick Pd islands on a Pd monolayer base. This conclusion follows from respective Pd and Mo Auger data which do not show sufficient change after 800K annealing to corroborate the above monolayer base interpretation. Peak areas of first CO desorptions $A_{\text{TPD}(1)}$ are plotted in Fig. 6b as normalized to the desorption peak area of the thickest, bulk-like Pd deposit at RT ($Q=12\text{ML}$). Both sets of data for RT deposits clearly establish the fact that bulk surface properties as determined by work function and CO adsorption measurements are approached at a thickness of approximately 3ML, the same results as previously found for Pd/W(110)⁸.

Although the first thermal desorption measurements employed with the above as-deposited RT layers of Pd cause a small annealing effect by short time heating to 550-600k (compare TPD(1) and TPD (2) curves of Fig. 7), more severe changes of the CO adsorption behavior were expected as a consequence of either continuing the TPD heating regime to increasingly higher maximum temperatures for successive desorption cycles (Fig. 7) or of subjecting the Pd deposit to 2 min anneals at increasing T_a inbetween desorptions (Fig. 8). What effect such different annealing treatments have on Pd deposits of 4.5, 6 and 12 ML deposits is demonstrated by TPD or Kelvin probe $\Delta\phi$ measurements in Fig. 7 and Fig. 8, respectively. (The main advantage of the highly sensitive and reproducible Kelvin probe measurements of the $\Delta\phi$ changes caused by CO adsorption being their direct comparability with adsorption data of other investigators whereas TPD sensitivities have to be carefully calibrated). It is obvious from both types of CO adsorption/desorption measurements that the adsorption behavior changes in a similar way upon

annealing as was found for the discontinuous island films: preferred elimination of high energy adsorption sites followed by drastic reduction of the adsorbed saturation amount of CO which is combined with a sharp reduction of desorption energy. As expected because of the greater continuity and thickness, these deposits exhibited a somewhat retarded deactivation behavior when compared to the Pd island films on MoO_x supports.

The higher information content of dynamic $\Delta\phi$ studies with the help of a good Kelvin probe arrangement is demonstrated in Fig. 9 with CO adsorption and desorption on a severely deactivated 6ML thick deposit of Pd. Regions of chemisorption and physisorption can be clearly distinguished and used to check and adjust the detailed scheduling of adsorption/desorption tests.

In the case of Pd islands on MoO_x it had been found (Fig. 4) that measurements can very sensitively detect small island rearrangements, but the high work function of the MoO_x substrate was dominating. Since in continuous layers thicker than about 3 ML the bulk Pd work function dominates for RT deposits, changes brought about by annealing should be more revealing in terms of Pd surface property changes. This is seen in Fig. 10 for a 4.5 ML thick deposit where the work function changes of the clean Pd adsorbent layer compared with the CO induced work function changes after 2 min annealing treatments at increasing temperatures T_a . The quasi-simultaneous decrease of $\Delta\phi^{\text{Pd}}$ and $\Delta\phi_{\text{max}}^{\text{CO}}$ is characteristic for all overlayer thicknesses studied (up to $\sim 12\text{ML}$), only the temperature regions where the steepest declines of $\Delta\phi^{\text{Pd}}$ were found depend somewhat on the as-deposited Pd layer thickness. As in the

case of Pd islands on MoO_x , the thicker deposits exhibit structural and chemisorption changes at correspondingly higher annealing temperatures. This is also evident in the behavior of substrate and overlayer Auger amplitudes as a function of T_a in Fig. 11 for 6 and 12 ML Pd deposits. This figure furthermore indicates the Pd p-p Auger amplitudes expected from continuous RT deposits of 1 to 4 ML thickness (according to calibrations similar to Fig. 1). When comparing with these thicknesses the Auger results of Fig. 11 - although not as sensitive to annealing treatments as $\Delta\phi^{\text{Pd}}$ - demonstrate that the drastic lowering of the Pd work function and the CO adsorption cannot be due to massive Pd island formation on a Pd base layer of appreciably less than 3 ML thickness. If the Auger data had been compatible with such thin base layers, the explanation for the drastic lowering of both the work function $\Delta\phi^{\text{Pd}}$ and the CO adsorption could easily be rationalized by the "thin layer effects" of Fig. 6a and 6b. However, considering the Auger results of Fig. 11, which also show stronger than expected Mo amplitude increases for the most strongly deactivating T_a region from 800-1000K, we feel compelled to interpret the overall results in a different way now. One possible explanation is the deactivation of the Pd surface by Mo substrate atoms which react with and diffuse through the Pd overlayers. This substrate/overlayer interaction is probably accompanied by some Pd surface roughening through Pd island formation on relatively thick Pd base layers (with $n > 3$ ML). The alloying characteristics of the Mo/Pd system³⁸ and the appreciably lower Mo bulk work function (4.9 eV) vs. the work function of bulk Pd (5.5 eV) are qualitatively consistent with this picture³⁹. Although some contribution to the lowering of the

work function of the Pd overlayer might also be expected from the roughening of the surface during layer break-up and 3-dimensional island formation upon annealing (Smoluchowski effect⁴¹). More specific LEED, AES, XPS evidence in support of the surface alloying hypothesis will be presented in a forthcoming study⁴⁰.

3. Comparison of Pd island deposits and layer deposits

Qualitatively the general deactivation behavior of both types of Pd deposits with respect to the adsorption of CO is the same: The higher and the longer the heat treatments the more drastic was the reduction of the total adsorbed amount during saturation exposures, and this was combined with the preferred elimination of high energy adsorption sites and with a lowering of the desorption energy for the remaining sites.

Not surprisingly the details of CO deactivation depended appreciably upon substrate species available, average deposit thickness, and the various heating schedules employed. A summary of these effects is presented in Fig. 12 in terms of CO desorption peak areas (for saturation exposures) as normalized to the peak areas for the 1st desorption from as-deposited layers. It can be seen that (a) island deposits deactivate easiest and therefore, also show the biggest differences between 1st and 2nd desorptions (curve 1), (b) dynamic TPD-anneals are shorter and, therefore, less deactivating than 2 min. steady-state anneals, and thinner layers deactivate more easily than thick ones (curves 2, 3) and (c) a small amount of intentional O contamination on the Mo substrate ($AA_{O} : AA_{Mo} = .06$) enhances the deactivation process under otherwise identical conditions (curves 3, 4). These results are all compatible with the proposed deactivation mechanism that involves diffusional mixing of substrate species (Mo or MoO_y) with the Pd overlayers, a process which is probably accompanied by microstructural

island rearrangements and overlayer roughening. Whether the substrate species are located on or below the Pd surface and why they reduce the activity of the Pd surfaces towards CO remains under investigation⁴⁰.

Concluding Remarks

In many respects the metal/support system Pd/Mo(110) is a very attractive model system for catalytic studies. From the point of view of performing well controlled measurements of surface processes that may be of basic interest in many catalytic systems in general and in strongly interacting metal/support systems in particular (the SMSI system Fe/TiO₂, which was recently studied in detail by Dumesic and collaborators and showed evidence for Ti deactivation of the Fe particle surfaces⁴², is a good example), the experimental situation for Pd/Mo(110) seemed rather ideal, and first results appeared promising. In the course of our efforts it became evident, however, that (1) the Pd island sizes which could be grown on MoO_x were larger than expected originally, (2) the MoO_x-c(14x7) oxide surfaces were not as non-reactive with Pd as anticipated, and (3) the clean Mo(110) support surfaces also interacted - perhaps alloyed - more strongly with Pd than expected. In summary, therefore, metal support interactions in the Pd/O/Mo(110) system were more significant than presumed initially.

This result has had the overall effect of complicating the experiments and their interpretations. On the other hand, however, this work should indicate a rather promising combination of powerful experimental techniques with which to investigate other metal support systems successfully.

In this way our experimental approach can be expected to make a contribution to solving the intriguing question of what constitutes

Page 17

MSI behavior.

Acknowledgements

The authors would like to thank E. Bauer for many discussions and a critical reading of the manuscript. C. P. acknowledges support of this work through NASA Grant NCC2-248.

Q (E.M.L)	Θ_{Pd} (%)	$\Lambda_{TPD(1)}$ (Å)	$\Lambda_{TPD}/\Theta_{Pd}$	$1/d$	l (nm)
10	100	100	1.00	-	-
6	60	74	1.23	17	36
3	48	55	1.16	25	36
2	36	45	1.24	32	-
1.5	-	38	-	-	-
1	23	24	1.04	93	-
.5	-	14	-	-	-

TABLE 1

References

1. G. M. Schwab, *Adv. Catal.* 27 (1978).
2. F. Solymosi, *Catal. Rev.* 1 (1967), 233
3. S. J. Tauster, S. C. Fung, R. T. Baker, J. A. Horsley, *Science* 211
13 March 1981, pg. 1121.
4. M. A. Vannice, R. L. Garten, *J. Catal.* 56 (1979) 236.
5. B. Imelik, C. Naccache, J. Coudurier, H. Praliand, P. Meriaudeau,
P. Gallezot, G. A. Martin, J. C. Vedrine (Eds.), *Metal-Support
and Metal-Additive Effects in Catalysis*, 1982, Elsevier Sci.
Publ. Co., Amsterdam.
6. G. C. Bond, B. Imelik et al (edits.), *Metal-Support and
Metal-Additive Effects in Catalysis*, Elsevier/Amsterdam, 1982, pg.
1.
7. S. L. Weng, M. El-Batanouny, *Phys. Rev. Lett.* 44, (1980), 612;
M. El-Batanouny, M. Strongin, G. P. Williams, J. Colbert, *ibid*,
46 (1981), 269.
8. D. Prigge, W. Schlenk, E. Bauer, *Surf. Sci.* 123 (1982), L 698.
9. H. Poppa, F. Soria, *Phys. Rev. B.* 27 (1983), 5166
10. M. El-Batanouny, D. R. Hamann, S. R. Chubb, J. W. Davenport, *Phys.*
Rev. B 27 (1983), 2575
11. K. Christmann, G. Ertl, *Surf. Sci.* 33 (1972), 254
12. K. Christmann, *Thin Solid Films* 46 (1977), 249
13. V. D. Vankar, R. W. Vock, B. C. DeCooman, *Thin Solid Films* 102
(1983), 313
14. H. Conrad, G. Ertl, J. Koch, E. E. Latta, *Surf. Sci.* 43 (1974),
462
15. A. M. Bradshaw, F. M. Hoffmann, *Surf. Sci.* 72 (1978), 513

16. T. J. Engel, J. Chem. Phys. 69 (1978), 373
17. J. J. Engel, G. Ertl, Adv. Catal. 28 (1979)
18. D. R. Loyd, C. M. Quinn, N. V. Richardson, Solid State Commun. 20 (1976), 409
19. M. P. Kisiknova, G. M. Bliznakov Surf. Sci. 123 (1982), 61
20. G. E. Rhead, Surf. Sci. 68 (1977), 20
21. R. L. Park, H. H. Madden, Surf. Sci. 11 (1968), 188
22. S. D. Bader, J. M. Blakely, M. B. Brodsky, R. J. Friddle, R. L. Panosh, Surf. Sci. 74 (1978), 405
23. M. Thomas, J. T. Dickinson, H. Poppa, G. M. Pound, J. Vac. Sci. Techn. 15 (1978), 568
24. D. L. Doering, H. Poppa, J. T. Dickinson, J. Catal. 73 (1982), 91
104
25. S. Ladas, H. Poppa, M. Boudart, Surf. Sci. 102 (1981), 151
26. K. Heinemann, T. Osaka, H. Poppa, Ultramicroscopy, to be published
27. H. Poppa, Ultramicroscopy, (1983)
28. C. Papageorgopoulos, H. Poppa, Proc. 4th Int. Conf. on Solid Surfaces and ECOS-3, Cannes, 1980, p. 688
29. H. Poppa, F. Soria, Surf. Sci. 115 (1982), L105
30. E. Bauer, T. Engel, Surf. Sci. 71 (1978), 695
31. F. Soria, H. Poppa, J. Vac. Sci. Technol. 17 (1980), 449
32. E. Bauer, H. Poppa, Thin Solid Films 12 (1972), 167
33. S. Ichikawa, Ph. D. Thesis, Stanford Univ. 1983
34. G. Ertl, J. Koch, Adsorption-Desorption Phenomena, F. Ricca editor, Academic Press, 1972, p. 345
35. E. Bauer, The Chemical Physics of Solid Surfaces and Heterogeneous Catalysis, D. A. King, D. P. Woodruff, eds., Vol. III, Elsevier Publ. Co., Amsterdam 1983

36. W. Schlenk, E. Bauer, Surf. Sci. 93 (1980), 9
37. D. Prigge, W. Schlenk, E. Bauer, Surf. Sci. 123 (1982), L698
38. R. P. Elliott, Constitution of Binary Alloys, McGraw-Hill, New York 1965
39. J. Holzl, F. K. Schulte, Solid Surface Physics, Vol. 85, Springer Verlag, Berlin 1979
40. C. Park, E. Bauer, H. Poppa, to be published
41. R. Smoluchowski, Phys. Rev. 60 (1941), 661
42. J. Santos, J. Phillips, J. A. Dumesic, J. Catal 81 (1983) 147

Figure Captions

Fig. 1: Room temperature growth of Pd on clean Mo(110) as a function of deposition time. Derivative peak to peak Auger amplitudes are plotted for a Pd deposition rate of 0.1 ML/min.

Fig. 2: Temperature programmed desorption of saturated (6L) CO exposures from Pd layers of varying average thickness Q (in equivalent monolayers, E.ML) on a MoO_x substrate. Traces (1) and (2) refer to the first two consecutive desorptions. The p-p Pd Auger amplitudes are given as determined after the first and second desorption; Mo/Pd are the respective substrate/ overgrowth Auger ratios.

Fig. 3: Saturated (6L) CO desorptions from 2 E. ML thick Pd layers on MoO_x substrates. Each freshly RT deposited Pd layer was pre-annealed at T_a for 2 min before the first CO dose and desorption.

Fig. 4: Change in work function ($\Delta\phi^{Pd}$) and p-p Auger amplitudes of a 3 E. ML thick Pd layer on a MoO_x substrate subjected to 2 min anneals at increasing temperature T_a .

Fig. 5: Change of p-p Auger amplitudes for a thick layer of Pd on a MoO_x substrate following successive anneals (2 min) at increasing T_a .

Fig. 6: (a) Work function change ($\Delta\phi^{Pd}$) of a Mo(110) surface covered by consecutive and cumulative deposits of Pd at RT, or by cumulative RT deposits annealed for 2 min at 800K after each deposit. (b) TPD peak areas of first saturated CO desorptions from Pd layers of increasing thickness Q deposited at RT on Mo(110); the peak areas were normalized to the desorption

Fig. 6: peak area from a thick (12ML) RT deposit (100%).

Fig. 7: TPD spectra of a 6 ML thick RT deposit of Pd subjected to consecutive 2 min anneals at increasing T_a .

Fig. 8: Kelvin probe work function measurements during the programmed thermal desorption of 6L of CO from a 12 ML thick and a 4.5 ML thick RT Pd deposit on Mo(110). After each desorption the Pd deposit was annealed for 2 min at increasing T_a .

Fig. 9: Example of kinetic work function measurements with a Kelvin probe; the adsorption and desorption process can be followed in detail.

Fig. 10: Change of the clean Pd work function ($\Delta\phi^{Pd}$) and of the work function induced by saturated CO exposures ($\Delta\phi_{max}^{CO}$) of a 4.5 ML thick RT deposit of Pd on Mo(110). The $\Delta\phi$ changes are monitored as a function of increasing annealing temperature T_a .

Fig. 11: Influence of increasing annealing temperature T_a (consecutive 2 min anneals) on the p-p Auger amplitudes of two continuous Pd layers of different thickness deposited onto Mo(110).

Fig. 12: Summary of CO deactivation caused by annealing of Pd deposits of varying thickness on MoO_x and Mo(110) substrates; (---, ~-) kinetic anneals by performing TPD to increasing maximum temperatures, (-.-, -) consecutive 2 min steady-state anneals.

All CO desorption peak areas (A_{TPD}) are normalized to the respective peak areas for the first desorption from as-deposited RT layers.

Table 1

Comparison of normalized TPD - measured surface areas of Pd deposits on MoO_x for Pd layers of varying thickness (Q). Some values for average Pd island lateral extension \bar{l} and thickness d which follow from assuming a simplified island morphology are also included.

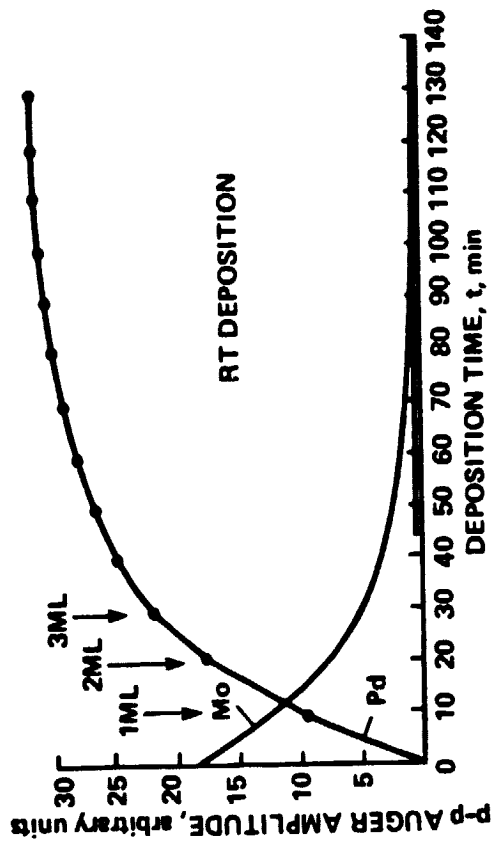


Fig. 1

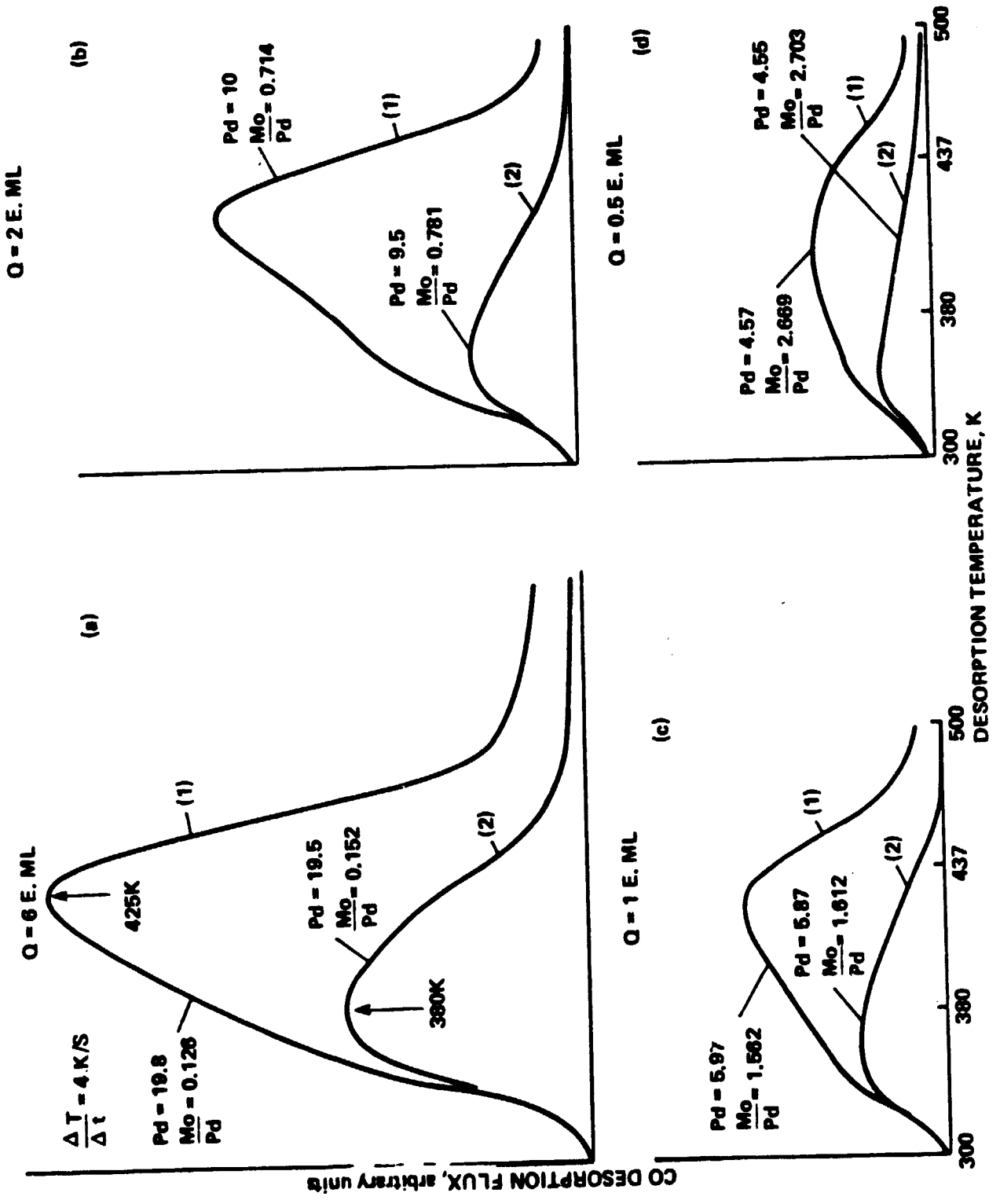
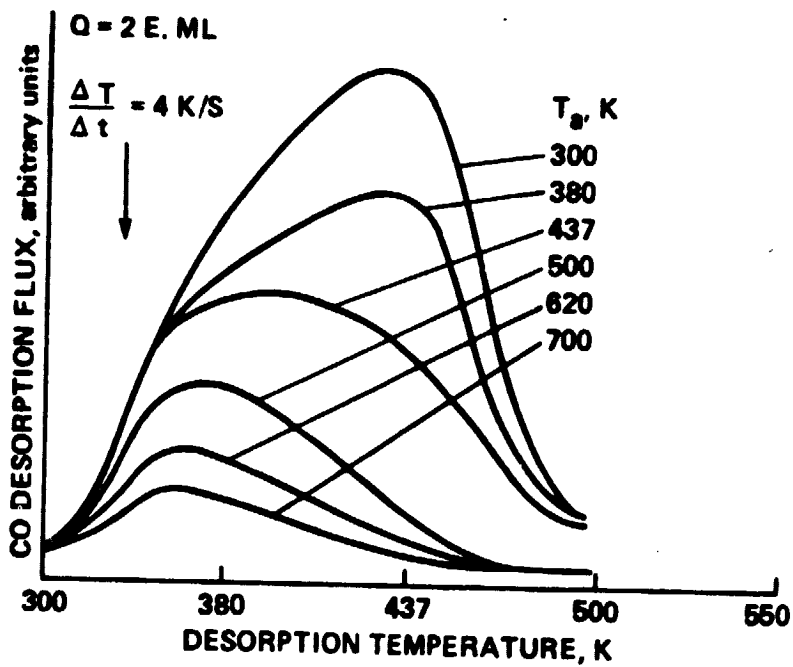


Fig. 2



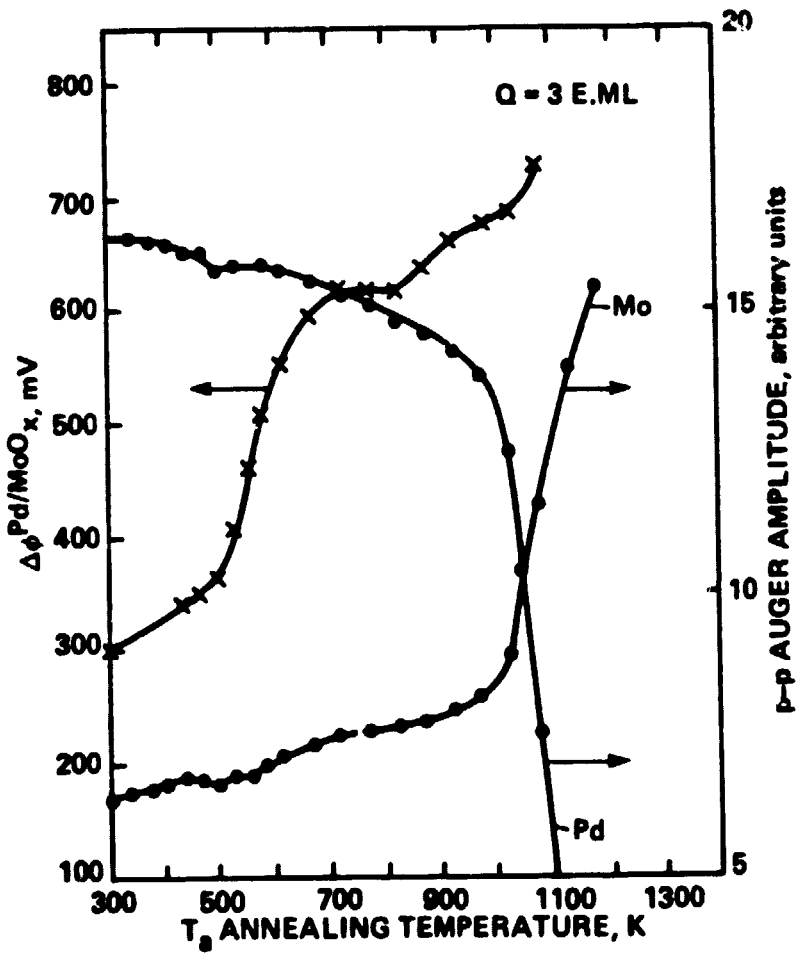


Fig 4

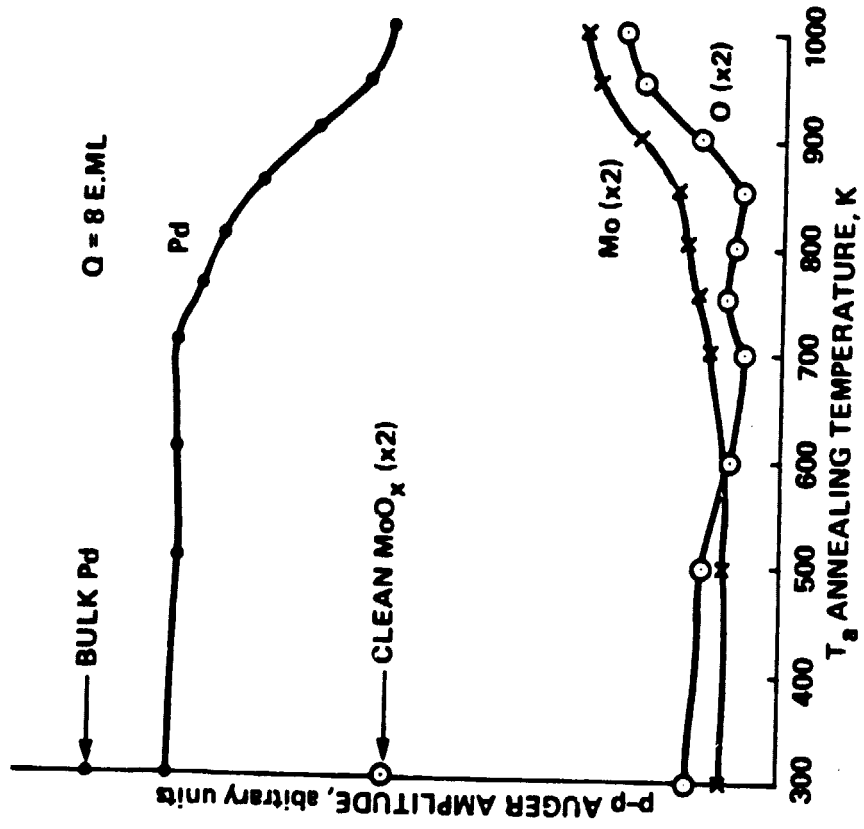


Fig. 5

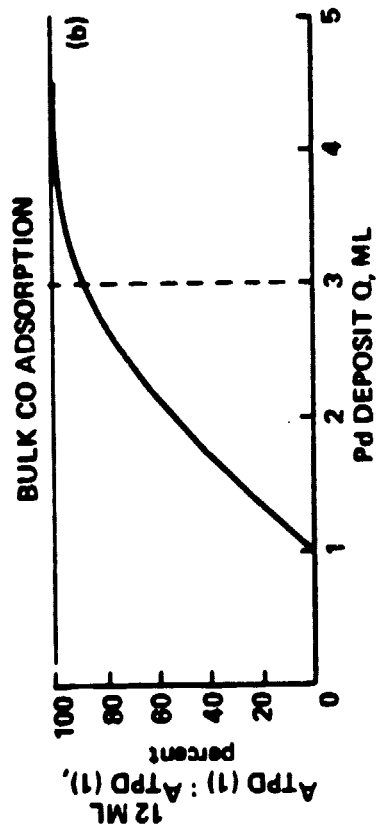
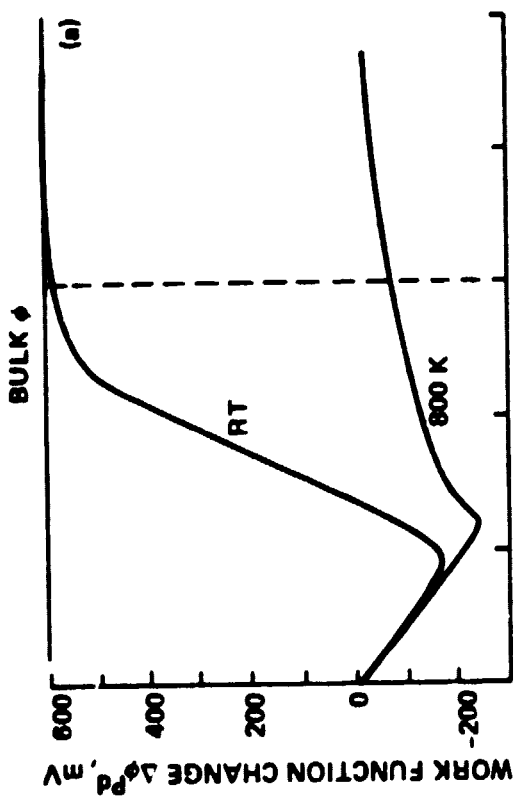


Fig. 6

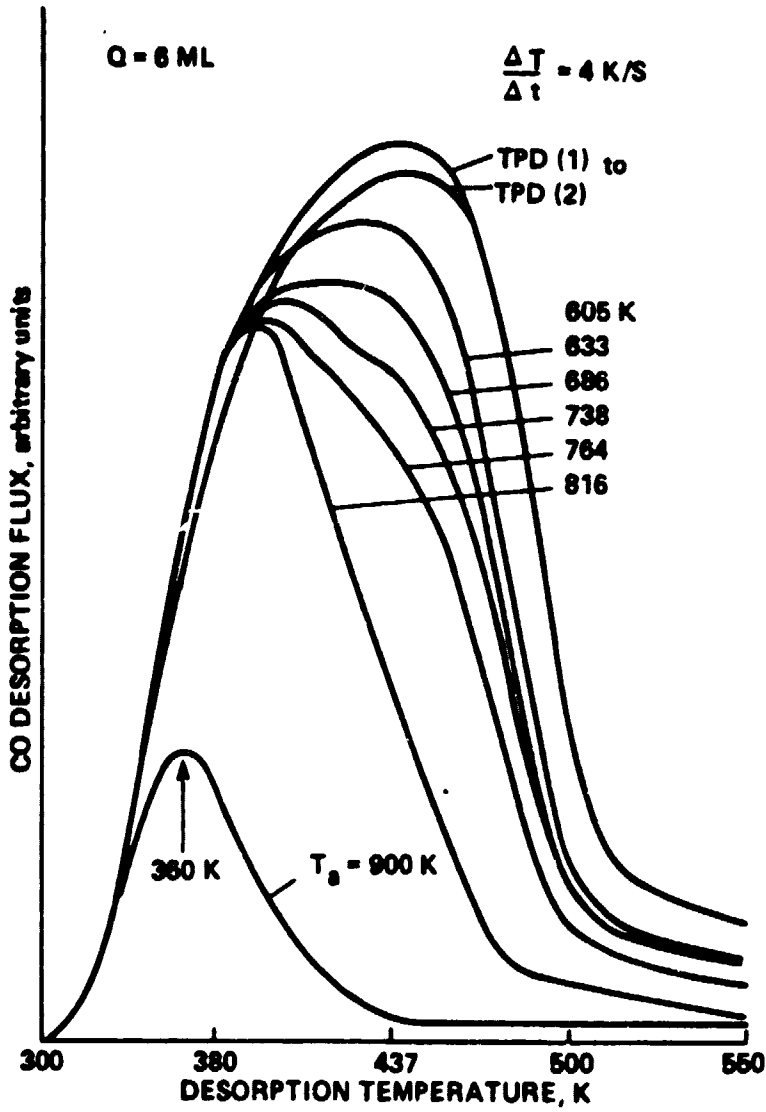


Fig. 7

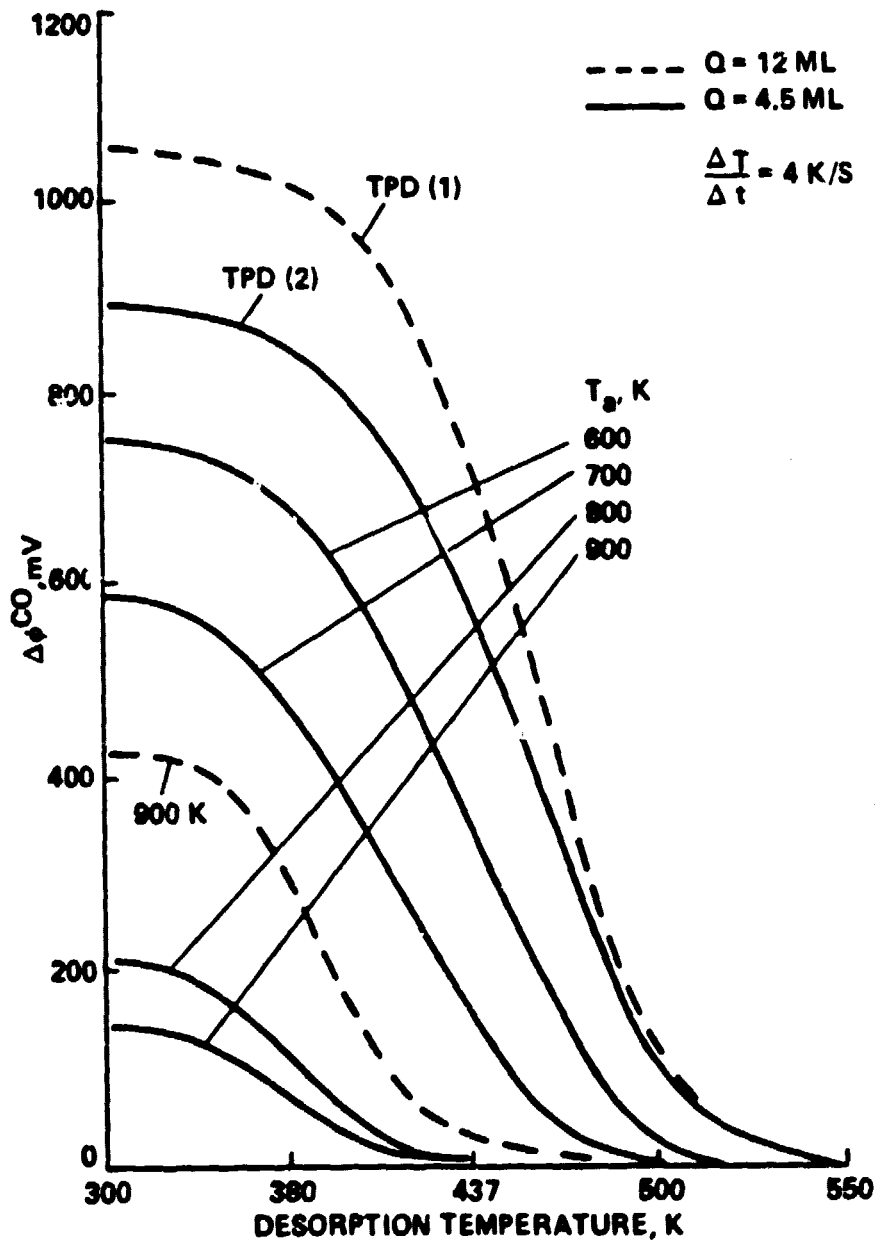


Fig 8

6 ML Pd/Mo (110)

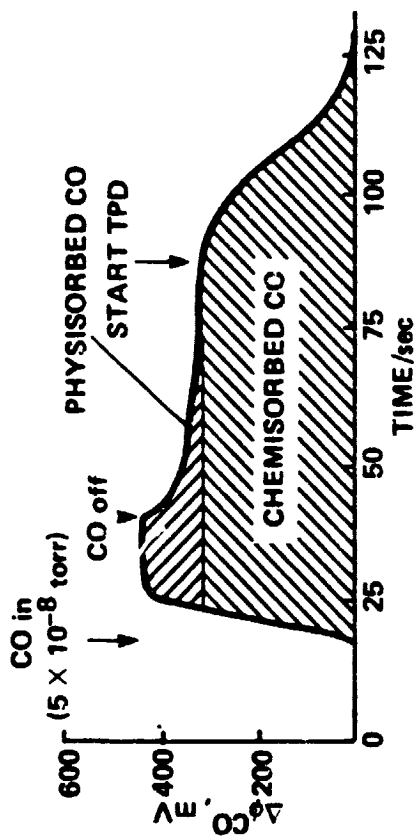


Fig. 9

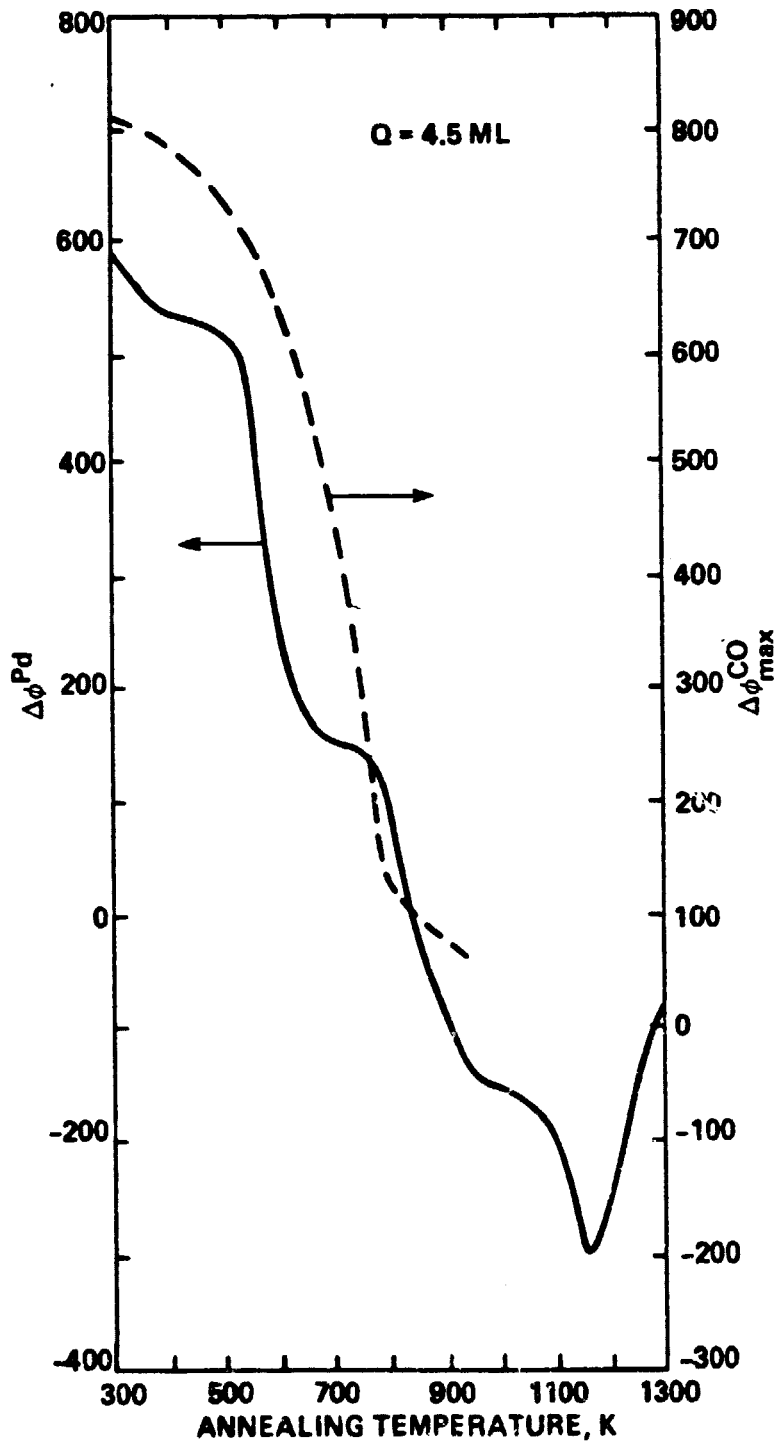


Fig. 10

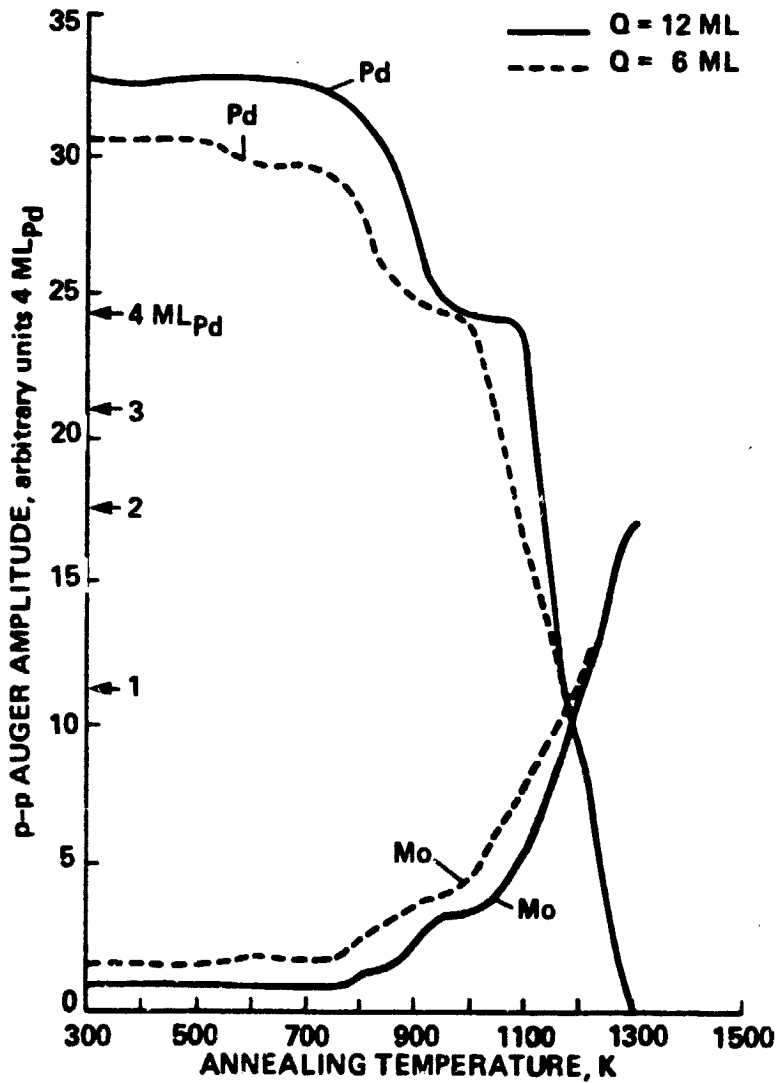


Fig. 11

APPENDIX 2

Growth and alloying of Pd films on Mo(110) surfaces

Ch. Park, E. Bauer* and H. Poppa

Stanford/NASA Joint Institute for Surface and Microstructure
Research, NASA Ames Research Center, Moffett Field, USA-CA 94035

The growth and annealing behavior of Pd on Mo(110) is studied in the thickness range from 0 to 12 monolayers at temperatures up to 1300 K using AES, XPS, LEED and work function change measurements. Similar to Pd on W(110), different growth modes are found at room and elevated temperatures. Dissimilar to Pd on W(110), the monolayer structure is different. Clear evidence for alloying is seen once the films are thick enough to remain continuous during annealing at temperatures up to 1100 K. At lower thicknesses the layers agglomerate during annealing. A model in which Pd-Mo alloy islands are surrounded by a distorted thin layer (1 - 2 ML) of Pd fits the results very well.

*Permanent address: Physikalisches Institut, Technische Universität
Clausthal, D-3392 Clausthal-Zellerfeld, Fed. Rep. of Germany.

1. Introduction

Alloying in small particles and in very thin films has recently received considerable interest in various fields of science and technology, for example in heterogeneous catalysis and in microelectronics. In the first field the problem appears in connection with the surface composition of bimetallic catalyst particles, in microelectronics the interdiffusion of contact materials on semiconductor substrates is of interest. In the past it has been generally assumed that alloying is insignificant up to temperatures at which volume diffusion sets in, extremely fine-grained films excepted in which a certain amount of mixing occurs due to grain boundary diffusion. Thus many epitaxy experiments of metals on metals with complete miscibility were performed at temperatures between 200 °C and 400 °C and analysed assuming no alloying. In particular, alloying was not suspected if the film material was not soluble in the substrate. In the present paper, which was stimulated by annealing-induced CO adsorption anomalies(1) on thin film surfaces, it will become evident that low temperature alloying can occur in thin films even if the substrate is a refractory metal and has very strong interatomic bonds as evidenced by a high sublimation energy, provided that the substrate is soluble in the film material. A good example of such a film-substrate combination is Pd on Mo. The solubility of Pd in Mo is very small at temperatures below 1000 K but Pd can dissolve slightly more than 40 atomic % Mo even at low temperatures(2). This system is of interest in model catalyst studies(1) and in microelectronics in which Pd and Mo are important contact materials. The (110) surface of Mo was chosen as substrate because this is the most densely packed surface which is expected to show the least alloying.

2. Experimental

The experimental setup and procedures have been described previously(1). The system was equipped with a double-pass cylindrical mirror analyser with integral gun, used for AES and XPS, LEED, quadrupole mass spectrometer, and a Kelvin probe with gold plated electrode for work function change ($\Delta\phi$) measurements. The base pressure was $6 - 7 \times 10^{-11}$ Torr and never exceeded 2×10^{-10} Torr during long time deposition of thick Pd layers. Pd was deposited by sublimation from resistively heated Pd wire at a rate of approximately 0.1 ML/min. The deposit showed no AES-detectable impurities. The (C(272 eV) + Pd(279 eV)) : Pd(330 eV) Auger peak ratio was used as a measure of carbon contamination; it was always smaller than 0.18 (for a modulation voltage of $2 V_{pp}$), which is 10 to 50 % lower than previously reported handbook values for 'clean' bulk Pd. The Mo(110) crystal, oriented to within 0.05° , was cleaned by heating in oxygen which was followed by repeated flashing to 2000 K until no carbon diffused to the surface during prolonged anneals at 1300 K. The AES data were recorded with typical beam parameters of 2 kV, 3.5 μ A and modulation voltages of 0.5 V_{pp} and 2 V_{pp} for Pd and Mo respectively. The XPS data were acquired employing a computerized data acquisition system with an energy resolution of about 0.5 eV. The temperature of the crystal was measured with a W-5%W-26%Re thermocouple and correlated with infrared and optical pyrometer readings.

3. Results

3.1 Room temperature deposition

3.1.1 AES results

The Auger peak-to-peak amplitudes (AA) of Pd at 330 eV and Mo at 179 eV are shown in fig. 1 as a function of the number of Pd doses at room temperature. The Pd AA increases linearly with rather well defined breaks at the completion of each layer, which is characteristic for two-dimensional layer-by-layer growth. The Mo AA decreases in a similar way. The slope ratio of the first two linear segments of Pd AA is $s_2/s_1 = 0.559$ averaged over several experiments. This ratio is quite similar to the value of 0.59 for the Pd/W(110) system(3). However, as shown in fig. 2a for a few selected Pd coverages, the derivative Pd Auger peaks showed considerable peak shape change, which can be clearly recognized by the changes in the resolution of the sub-peak of the 330 eV Pd peak. The peak-to-peak height of the "S-peak" as shown in the insert of fig. 1a which is characteristic for this resolution is plotted as a function of Pd doses in fig. 1a. Within the limits of error the S-peak increases proportional to the main Pd peak up to 1 ML and then decreases to a minimum at about 2 ML. Thereafter it shows again a slight increase which is proportional to that of the main Pd peak. As can be seen in the numerically integrated $N(E)$ curves (fig. 2b), the S-peak changes are due to changes in the $M_{4,5}N_{4,5}N_{4,5}$ doublet structure. The low energy peak shows a considerable shift (about 0.85 eV at 3 ML) toward higher energy between 1 ML and 2 ML. Because of this shape change with coverage, some of the derivative AES data were numerically integrated. Fig. 1b shows the area under the integrated

Pd Auger signal (fig. 2b) as a function of the Pd AA. The data of fig. 1b are normalized at 3 ML to the Pd AA because at this coverage no further significant shape changes are seen so that negligible deviations are expected. It is found that the AA is 11 % larger than the area under the Auger peak at one monolayer thickness. In the second monolayer this difference decreases to zero. When the integrated $N(E)$ Auger peak areas are plotted as a function of Pd dose (analogous to fig. 1a) a slope ratio of 0.690 is obtained for the first two linear segments. Assuming the growth of (111) planes of Pd layers with bulk spacing of $d(111) = 2.25 \text{ \AA}$, an inelastic mean free path length of $\lambda = 8.16 \text{ \AA}$ is obtained for the 330 eV Pd Auger electrons. This value agrees well with $8.2 \text{ \AA}(4,5)$ for Ag (351 eV Auger electrons) and is more reasonable than the value $\lambda = 5.8 \text{ \AA}$ obtained from the derivative Auger peaks considering the general energy dependence of the inelastic mean free path of electrons in solids(6).

3.1.2 XPS measurements

X-ray photoemission spectra of the Pd and Mo 3d core levels and of the respective valence bands were recorded. Fig. 3 shows the Pd 3d core level spectra of Pd layers deposited at room temperature for several coverages. The Pd 3d peaks for 12 ML are very asymmetric. The asymmetry decreases gradually as the thickness of Pd decreases and the peaks shift to higher binding energy from the approximately bulk Pd binding energy at 12 ML (referenced to the clean Mo 3d core levels). The shift of 0.4 eV is about the same for 2 ML and 0.7 ML but the asymmetry is still smaller at 0.7 ML than at 2 ML. The 0.7 ML spectra differs from the 2 ML and 12 ML spectra in still another respect: the FWHM of the peaks is only about 80 % of that at 2 ML

and 12 ML. The 3d peak asymmetry is generally related to the density of states at the Fermi level(7). The observed valence band spectra are consistent with the above trend: With increasing Pd thickness, a broad band with a sharp Fermi edge gradually develops. In the 12 ML thick Pd layer distinct satellite structure at about 6 eV below the Pd $3d_{3/2}$ peak was observed, which was absent in thin layers. This satellite peak can be attributed to a 4d-valence electron shake-up process(8). It is also consistent with the evolution of the valence band in the thick layer. The Mo 3d core levels are approximately symmetric and the binding energy is independent of the Pd thickness. The relative intensities of the Mo $3d_{5/2}$ peaks for various Pd overlayer thicknesses were used to calculate the inelastic mean free path of these electrons (1026 eV electron energy). A value of $\lambda = 18 \text{ \AA}$ is obtained which agrees well with literature values(9).

3.1.3 LEED measurements

The LEED patterns observed during the growth of Pd layers at room temperature are quite similar to those of Pd on W(110) (3). Therefore, only the important features will be discussed. Up to one monolayer the RT deposits show an unsharp (1x1) structure with considerable background; the layer is pseudomorphic. With increasing Pd dosage, the unannealed Pd deposits show, in addition to the (1x1) pattern, extra spots which can be attributed to a somewhat distorted Pd (111) plane. At 12 ML the distorted (111) structure has approached a nearly perfect hexagonal Pd(111) bulk structure. The alignment of the Pd(111) layer relative to the Mo(110) surface follows the Nishiyama-Wassermann (NW) orientation relationship, Pd(110)/W(001).

3.1.4 Work function measurements

The work function change ($\Delta\phi$) upon Pd deposition at room temperature is shown in fig. 4. Similar to Pd on W(110), the work function decreases initially, passes a minimum, increases monotonically with further two-dimensional layer growth and saturates rapidly at around 3 ML. The minimum of the work function occurs at the coverage at which the first layer is completed. The saturation work function change of $\Delta\phi = 600$ mV agrees well with the work function difference between bulk Pd(111) (5.55 eV(10)) and Mo(110) (4.95 eV(11)).

3.2 Deposition at elevated temperatures

The Pd deposits on heated substrates show a different growth mode. Pd condensed in excess of 1 ML tended to form three-dimensional crystals at temperatures as low as 550 K. Furthermore, Pd starts to alloy with the substrate at temperatures above 750 K as will be discussed in the next section. Fig. 5 shows the Pd AA as a function of the number of 2 min Pd doses at 700 K. The linear increase of the Pd AA in the first segment has the same slope as that of room temperature deposits and indicates two-dimensional growth of the first layer and no alloying. The slope ratio of $s_2/s_1 = 0.2$ is, however, much smaller than for RT growth ($s_2/s_1 = 0.559$) which indicates formation of three-dimensional crystallites on top of the first monolayer. The S-peak height also behaves quite differently from RT deposits after completion of the first layer. Instead of rapidly decreasing to small values, the S-peak decreases only slightly to about 80 % of its maximum value. This is compatible with the formation of crystallites which contribute only a little to Auger amplitude and S-peak height.

The LEED patterns obtained during deposition at 300 K and 700 K differ considerably (fig. 6). At coverages below 1 ML, Pd deposition at 700 K produced the "complex pattern" shown in fig. 6a. The same pattern is obtained by annealing of room temperature deposits of similar thickness above 700 K. This structure was not seen in Pd on W(110) and may be considered as a distorted Pd(111) plane (see sec. 4). Further deposition (at 700 K or at 300 K followed by annealing above 700 K) leads to additional incorporation of Pd into the first layer and the "complex pattern" is replaced completely by a (1x1) pattern when approaching an ideal 1 ML. Above 1 ML, a (3x1) structure (fig. 6b) develops and improves in quality and intensity with thickness. This structure was also observed in the Pd/W(110) system and was interpreted as a distorted Pd(111) plane with the same saturation density as a (1x1) structure(3). In addition to the (3x1) spots, extra spots close to the Mo spots appeared at the same time (fig. 6b). They are due to epitaxial Pd(111) crystals in Kurdjumov-Sachs (KS) orientation(3). The extra spots increase in intensity with increasing Pd thickness until they are the only spots seen (fig. 6c, 12 ML). Pd layers annealed at higher temperature (1000 K) after each dose show similar patterns. However, the (3x1) pattern is much less developed than in the layer annealed at 700 K and did not increase in relative intensity after about 20 min doses. In contrast to the (3x1) structure spots, the intensity of the epitaxial Pd spots increased continuously, which indicates lateral growth of Pd(111) crystals. The coexistence and independent behavior of these two structures indicates that Pd condenses as three-dimensional crystals which are surrounded by a thin Pd layer with (3x1) structure.

The work function changes ($\Delta\phi$) upon Pd deposition at elevated temperature (e.g. at 700 K), or upon Pd deposition at room temperature which was followed by annealing after each dose (at 800 K and 1000 K, fig. 4), also indicate three-dimensional growth. Since the Kelvin probe measures the average work function, the measured $\Delta\phi$ represents an area average over regions covered by the initial two-dimensional layer (1 - 2 ML) and regions covered by three-dimensional crystals with the bulk work function of Pd(111). In this simple picture the total area covered by three-dimensional crystals can be estimated:

$$\phi_{av} = A_{111} \phi_{111} + (1 - A_{111}) \phi_{base}^{(1 - 2 \text{ ML})},$$

where A_{111} is the fraction of the surface covered by the Pd(111) crystallites with work function $\Delta\phi = 600$ mV and $(1 - A_{111})$ the area fraction covered by the monolayer ($\Delta\phi = -250$ mV) or by the double layer ($\Delta\phi = 300$ mV). The measured $\Delta\phi$ values of the Pd layer annealed at 800 K might be explained by crystallites on a monolayer base with total area coverage of about 25 % after 40 one min doses (equivalent to 4 ML average thickness). The $\Delta\phi$ value of a deposit annealed at 1000 K would require a surface coverage by crystallites of less than 10 % on a 1 ML base for 4 equivalent monolayers of Pd deposition. This disagrees with the LEED observation that the epitaxial Pd(111) structure is dominating at this coverage which indicates a high surface coverage by Pd(111) after annealing at 1000 K. The saturation of the (3x1) structure at a coverage as low as 2 ML also disagrees with this simple coalescence picture. It is even more difficult to explain the $\Delta\phi$ values by assuming crystallites on a 2 ML thick base layer. These observations lead to the hypothesis that alloying occurs upon deposition or annealing at high temperature (> 800 K). This hypothesis will be examined in more detail in the next section.

3.3 Annealing

3.3.1 Thick layer (12 ML)

In order to understand more about the film structure and the possibility of alloying, thick (12 ML) Pd layers were grown at room temperature and annealed for 2 min at stepwise increasing temperatures. The changes of the Pd and Mo Auger amplitudes and of $\Delta\phi$ are presented as a function of annealing temperature in fig. 7. No significant changes in Pd and Mo Auger signals occur up to 750 K. Above 750 K, the AA of Pd decreases rapidly to a plateau between 950 K - 1090 K. This is followed by a rapid decrease above 1100 K with the onset of Pd desorption. Complementary changes are seen in the AA of Mo.

The work function changes seen at temperatures below 500 K were due to the desorption of small amounts of gases (CO) adsorbed during the waiting period from the residual background vacuum. The slight increase in work function seen at 600 K may possibly be associated with minor annealing of surface defects. The work function decreases drastically from 750 K to 940 K, which is followed by a minor drop to 1090 K. Further changes above 1100 K are due to desorption and are the reverse of the $\Delta\phi$ changes seen during deposition in the monolayer range. The first Pd AA drop at 750 K is accompanied by a drastic decrease of the work function to 60 mV. This would correspond to the work function of a very thin layer (less than 2 ML), which would suggest massive coalescence into three-dimensional crystallites. However, the LEED and the Auger observations do not allow such a simple interpretation. The LEED pattern of the Pd(111) layer in NW orientation seen before annealing showed, surprisingly, no change upon annealing up to 1090 K. No changes in spot spacing, sharpness,

and intensity and no noticeable changes in the background intensity could be observed. Only above 1100 K does the LEED pattern change (fig. 9a): Mo(1x1) spots start to become visible in addition to the Pd(111) structure, which indicates the onset of agglomeration and possible desorption. This is followed by the disappearance of the Pd(111) spots and the transition to the "complex pattern" at a coverage of less than one monolayer (1200 K). Because LEED and AES show no evidence of massive agglomeration upon annealing up to 1090 K (and no detectable impurities are found on the surface), the drastic change of $\Delta\phi$ and of the Auger amplitude can only be explained by alloying causing considerable diffusion of Mo into the Pd layer. This picture is compatible with the bulk Pd-Mo phase diagram: the solubility of Pd in Mo is very small at temperatures below 1000 K but Pd dissolves more than 40 atomic percent of Mo at low temperatures(2). XPS measurements were performed before and after the drastic work function drop of fig. 7. Fig. 8a shows Pd 3d core level spectra of a 12 ML thick Pd deposit before and after annealing at 1000 K. Annealing up to 700 K did not change the Pd 3d peak. However, after a 1000 K anneal, the 3d peaks shift significantly to higher binding energy by about 0.7 eV. Simultaneously, the large asymmetry of the line shapes of the unannealed film is considerably reduced. The satellite peak on the high energy side of the $3d_{3/2}$ line ($E = 6$ eV) also has disappeared after annealing at 1000 K. The valence band spectra also show a significant change upon annealing (fig. 8b). The sharp Fermi edge of the unannealed film, which is similar to that reported for valence spectra of bulk Pd(6), recedes to higher energy. Changes similar to our XPS observations were reported for a number of bulk Pd alloys (Pd-Ag(12), Pd-Cu(13,14)). Although Mo 3d core levels did not show a change in binding energy or line shape, they showed a significant intensity increase by a

factor of 2.2. These XPS results and the fact that the Pd layer is still continuous at this annealing temperature, strongly support the hypothesis of Mo diffusing into and alloying with Pd.

3.3.2 Thin layer (1 ML)

In order to understand the alloying process during annealing, Pd layers of various thicknesses were studied. First one extrem of thickness, i.e. the monolayer (1.06 ML) was examined. Fig. 10 shows the Auger amplitude of Pd and Mo as a function of annealing temperature. The Pd (Mo) Auger AA shows only a slight increase (decrease) upon annealing up to 950 K. This small change might be attributed to the smoothening and incorporation of small amounts of Pd in excess of 1 ML into the first layer as mentioned in sec. 2. Beyond 950 K, a slight decrease of the Pd AA was noted which was followed by a rapid decrease of the Pd AA and increase of the Mo AA due to Pd desorption. A slow increase of the Pd "S-peak" can also be seen, saturating at about 750 K, which is compatible with smoothening and further incorporation of small amounts of Pd into the first layer.

These results indicate that in the case of a monolayer no evidence of Mo diffusing into the top Pd layer was found so that the possibility of forming a two-dimensional surface alloy by place exchange with substrate atoms can be excluded. This is consistent with the surface free energy consideration; the Mo surface with high surface free energy (2.28 J/m²) (15) tends to remain covered by low surface free energy Pd (1.63 J/m²) (15).

3.3.3 Layer of intermediate thickness (3.5 ML)

In contrast to the two extreme thickness cases (12 ML and 1 ML), Pd layers in the intermediate thickness range deposited at RT undergo severe changes in layer structure upon annealing. At 3.5 ML thickness, the major changes in the Auger amplitudes and in $\Delta\phi$ can be divided into three stages as shown in fig. 11. The first stage starts at 600 K. Pd AA and Mo AA change rapidly to plateaus and the work function drops drastically (by about 500 mV). A slight increase of the S-peak can be also seen in this stage. A second stage of transformation begins at about 780 K: the Pd AA and $\Delta\phi$ decrease and the Mo AA increases. A further pronounced change of $\Delta\phi$ sets in at 930 K (3rd stage), at which temperature the desorption of Pd starts.

The LEED patterns of 3.5 ML thick Pd layers during annealing are quite similar to those of a 5 ML Pd layer (see sec. 3.3.4). In addition to the Pd "(111)" spots, the (3x1) structure spots develop right after the first work function drop is nearly completed (at about 710 K). The intensity of the (3x1) structure spots then increases with annealing temperature, is strongest at 850 K (fig. 9c), and is visible up to 980 K, i.e. up to temperatures when some Pd has already been desorbed. Upon annealing beyond 980 K, the (3x1) structure disappears (fig. 9d) and transforms to (1x1) and finally the "complex pattern" (fig. 9e) is obtained in the submonolayer range. For a Pd coverage range of less than 3.5 ML but greater than 1 ML, for example 1.65 ML which was studied in detail, the general annealing behavior was quite similar. However, the first and second stage were not well separated so that the drastic $\Delta\phi$ and Pd AA decreases and the development of the (3x1) structure were observed

earlier (650 K). The first transformation stage can be easily attributed to the simple coalescence and breaking up of a continuous layer. This is in agreement with observation that the Mo LEED intensities increase significantly relative to the Pd intensities in the first transformation stage. The second transformation stage may be associated with Mo diffusion and alloy formation. The strong increase of the Mo AA and the gradual development of the (3x1) structure, which is assumed to be an alloy structure, favor this interpretation.

3.3.4 Layer of intermediate thickness (5 ML)

With further increasing thickness, the changes in the first annealing stage become weaker and those in the second stage more pronounced. Fig. 12 shows the annealing behavior of a 5 ML thick Pd layer. The first stage begins here at 550 K. The Pd AA drops only slightly and the $\Delta\phi$ changes are relatively small compared to the 3.5 ML case. The slight decrease of $\Delta\phi$ below 500 K was again due to small amounts of CO desorption. In the second stage, which starts at about 770 K, the work function and the Pd AA decreases and the Mo AA increases drastically towards a plateau region. The LEED patterns (fig. 9) were already described above. The (3x1) structure with superimposed Pd "(111)" spots appeared right after the first transformation stage was completed and gradually saturated around 850 K (fig. 9c). The next drastic change at 980 K is due to the onset of Pd desorption.

4. Discussion

4.1 Low coverages $\theta < 1$ ML

The first Pd layer on Mo(110) grows two-dimensionally quite similar to Pd on W(110). However, unlike Pd/W(110), less than a monolayer of Pd on Mo(110) showed a different LEED structure after annealing ("complex structure", see fig. 13a). This structure was observed at various coverages $\theta < 1$ ML and was independent of the way this coverage was established. This indicates island formation of a structure which may be considered a distorted Pd(111) plane (the reciprocal lattice unit mesh is shown in fig. 13a). The Pd-Pd distance in the Mo [001] direction is increased to fit the Mo periodicity and the Pd atom rows are parallel to the most densely packed Mo $[\bar{1}11]$ atom rows. The angle between the unit mesh vectors differs only by 2.8° from the substrate unit mesh angle and is, therefore, still far from 120° . This structure was present in two equivalent azimuthal orientations: Pd(111)//Mo(110), Pd $[\bar{1}10]$ //Mo $[\bar{1}11]$, $[1\bar{1}1]$ (Kurdjumov-Sachs orientation relationship) with an ideal saturation density of 1.40×10^{15} atoms/cm² which corresponds to a coverage $\theta = 0.98$ with respect to the Mo(110) plane.

Unlike the thicker Pd layers, there is no evidence of Mo diffusion or surface alloying at a thickness of one monolayer or less. This is understandable considering the appreciable difference in surface free energies of the two metals(15). The absence of alloy or compound formation up to a monolayer is reported for a number of alloying metal systems provided that the substrate material has a higher surface free energy than the adsorbate material, such as Pb on Au(16,17) and Au on Si(18). The AES line shape changes in the monolayer range are an immediate consequence of the reduced coordination

of the Pd atoms. Up to 1 ML each Pd atom has at most 6 Pd neighbours. During the formation of the second layer the percentage of Pd atoms which have only 6 Pd neighbours decreases and attains 9 neighbours at 2 ML. This increase in coordination and the accompanying transition in electronic structure from the $(4d)^{10}$ configuration of the free Pd atom to that of bulk Pd produces a broadening of the Pd 4d levels similar to, but larger than the broadening for the Pd 3d core levels seen in XPS spectra (fig. 3). Due to increasing broadening of the $4d(N_{4,5})$ levels of Pd above 1 ML, the $M_{5N_{4,5}N_{4,5}}$ and $M_{4N_{4,5}N_{4,5}}$ Auger transitions become broader so that the $M_{4,5N_{4,5}N_{4,5}}$ doublet becomes less resolved (decrease of the "S-peak"). In the submonolayer range, the resolution is constant because Pd forms islands already at low coverages and consequently the coordination does not change significantly with coverage. In addition to their different Pd-Pd coordination, Pd atoms in the submonolayer range differ from those in the bulk in their electronic structure because of their contact with Mo atoms. This can be seen in their drastically different adsorption behavior of the Pd monolayer: a Pd monolayer on Mo(110) does not adsorb CO(1).

4.2 Thick films

The LEED structure of 12 ML thick film shows the bulk Pd spacing within the limits of experimental error. Similar to Pd on W(110), the alignment of the Pd(111) plane relative to Mo(110) is $Pd[\bar{1}10] // Mo[001]$ (Nishiyama-Wassermann relationship) when deposited at 300 K, and $Pd[\bar{1}10] // Mo[\bar{1}11], [1\bar{1}1]$ (Kurdjumov-Sachs relationship) when deposited at 700 K. It is interesting that the thick layer is stable upon annealing up to 1090 K whereas thinner layers agglomerate at low temperature (stage 1). This may be so because too much material

is present in the thick layer so that coalescence is kinetically limited at the low temperature of stage 1. During the growth of thick epitaxial layers the strain energy may also be released by structural rearrangements toward the ideal Pd(111) layer. The thick layer remains continuous up to the onset of desorption. This may be explained by Mo diffusion into the layer, which stabilizes the structure against coalescence. The experimental results clearly show that Mo diffusion into thick layer commences upon annealing beyond 770 K. The composition of this layer which depends on annealing temperature and time can be estimated from the Auger amplitudes of Pd and Mo. The XPS intensities of Pd and Mo core levels provide another possibility for composition calculation. The Auger amplitudes of Pd and Mo on the well defined plateau at 1000 K (see fig. 7) are used to calculate the composition. When considering only some idealized and physically reasonable situations, a model structure (fig. 14) of the composition Pd₂Mo with a monolayer of Pd on top fits the measured Auger amplitudes and XPS intensities well. The Pd₂Mo phase has been reported for bulk Pd-Mo alloys(2,19). The actual layer composition may again be kinetically limited so that the Pd layer starts to agglomerate and desorb above 1090 K before Mo saturates the Pd film to the maximum solubility limit of 40 - 47 % Pd(2). The presence of a monolayer of Pd on top of this alloy structure is also compatible with surface free energy considerations.

4.3 Intermediate thickness region

Room temperature deposits of intermediate thickness are unstable and can only exist due to kinetic limitations. This is clear from LEED observations which definitely show two separate phases developing with increasing annealing temperature ((3x1) and Pd(111)).

The heterogeneity of the layer structure leads to a picture for the alloying process in which the layer first agglomerates (stage I), and then forms three-dimensional alloy crystals (stage II). The onset temperature of stage I depends on the thickness of the layer. Agglomeration starts earlier for thicker films: 650 K at 1.65 ML, 600 K at 3.5 ML, 550 K at 5 ML, and this may be due to increasing strain energy in thicker films. Towards the end of the first stage, the (3x1) structure starts developing and is strongest at about the middle of the second stage. The gradual evolution, saturation, and subsequent weakening of the (3x1) structure with increasing annealing temperature and with increasing Mo Auger amplitudes suggest that this structure is coupled with alloy formation. The lattice constant of the Pd-Mo alloys are independent of composition so close to Pd (e.g. $a = 3.89 \text{ \AA}$ for $\text{Pd}_2\text{Mo}(19)$ vs. $a = 3.8898 \text{ \AA}$ for bulk Pd) that it is not possible to distinguish the alloy from pure Pd by LEED. The driving force for alloying in the (3x1) structure is not only the heat of mixing but also the reduction of strain energy in the Pd layer by incorporation of Mo. Fig. 13b shows the reciprocal lattice unit mesh of the (3x1) structure which was also chosen for Pd on W(110) (3). Detailed examination of the intensity of the (3x1) spots during growth suggests that the (3x1) layer may be as thin as 2 ML. The alloy layer model for intermediate thickness is shown schematically in fig. 14b. The Auger intensity calculation at the temperature at which the (3x1) structure is best developed shows reasonable agreement with this model. An idealized composition of Pd_3Mo for the alloy island covered by a Pd monolayer and a surrounding (3x1) layer consisting of a monolayer of Pd_2Mo which is also covered by a Pd monolayer fits the Auger intensities well. A relative area coverage of alloy island of 30 to 70 % can be estimated for various thicknesses.

5. Summary

The growth and annealing behavior of Pd layers on a Mo(110) substrate is studied. The results can be summarized as follows: 1.) Similar to Pd on W(110), Pd forms a monolayer without alloying but the LEED structure in the submonolayer range is different from Pd/W(110) after heating to 700 K. 2.) In thick layers (12 ML) which were annealed above 770 K, clear evidence for Mo diffusion into the Pd layer and alloying has been seen. Such layers remained continuous up to 1100 K. 3.) Thinner Pd layers are less stable and start coalescing into crystallites upon annealing between 550 - 650 K (depending on thickness) and form above 770 K Pd-Mo alloy island covered by a Pd monolayer and surrounded by a Pd monolayer-covered alloy monolayer. 4.) Significant changes in Pd Auger peak shape as well as shifts of Pd core levels are observed during layer growth and annealing.

Acknowledgements

This work was performed under NASA Grant No. R05-030-001 and NCC 2-248.

References

- 1 Ch. Park, F. Soria and H. Poppa, *Thin Solid Films*, to be published.
- 2 F.A. Shunk, *Constitution of Binary Alloys*, 2nd Suppl., McGraw-Hill 1969, p. 520.
- 3 W. Schlenk and E. Bauer, *Surface Sci.* 93 (1980) 9.
- 4 E. Bauer, H. Poppa, G. Todd and P. Davis, *J. Appl. Phys.* 48 (1977) 3773.
- 5 P.W. Palmberg and T.N. Rhodin, *J. Appl. Phys.* 39 (1968) 2425.
- 6 M.P. Seah and W.A. Dench, *Surface and Interface Analysis* 1 (1979) 2.
- 7 S. Hüfner, G.K. Wertheim and D. Buchanan, *Chem. Phys. Lett.* 24 (1974) 527.
- 8 N. Martensson, R. Nyholm and Johansson, *Phys. Rev. Lett.* 45 (1980) 754.
- 9 C.R. Bundle, *J. Vac. Sci. Technol.* 11 (1974) 212.
- 10 H.B. Michaelson, *J. Appl. Phys.* 48 (1977) 4729.
- 11 S. Berge, B.O. Gartland and B.J. Slagsvold, *Surface Sci.* 48 (1974) 275.
- 12 P. Weighman and P.T. Andrew, *J. Phys. C., Solid State Phys.* 13 (1980) L821.
- 13 V.S. Sundaram, M.B. de Moraes, J.D. Rogers and G.G. Kleiman, *J. Phys. F., Metal Phys.* 11 (1981) 1151.
- 14 N. Martensson, R. Nyholm, H. Calen, J. Hedman and B. Johansson, *Phys. Rev. B* 24 (1981) 1725.
- 15 W.R. Tyson, *Can. Metall. Quat.* 14 (1975) 307.
- 16 J. Biberian, *Surface Sci.* 74 (1978) 437.
- 17 A.K. Green, S. Prigge and E. Bauer, *Thin Solid Films* 52 (1978)

18 A.K. Green and E. Bauer, Surface Sci. 103 (1981) L127.

19 D. Prigge, W. Schlenk and E. Bauer, Surface Sci. 123 (1982) L698.

20 A. Maldonado and K. Schubert, Z. Metall. 55 (1964) 619.

Figure Caption

- Fig. 1 a) Pd and Mo amplitude and "S-peak" height (see insert) as a function of Pd doses (1 dose = 1 min). b) Peak-to-peak Auger amplitude versus integrated Pd Auger peak area under $N(E)$ in fig. 2b.
- Fig. 2 a) Derivative MNN Auger spectra for Pd coverage ranging from zero to 3 ML illustrating significant variation of peak shape with coverage. $E = 2$ kV, $I = 3.5$ A, $V_{\text{mod}} = 0.5 V_{\text{pp}}$. b) Integrated Pd MNN spectra after subtraction of a linear background correction. Each curve corresponds to an increase of 2 min doses of Pd, Pd coverage range: zero to 3 ML.
- Fig. 3 XPS spectra for Pd 3d core levels for various thicknesses. a) 0.7 ML, b) 2 ML, c) 12 ML, deposited at room temperature.
- Fig. 4 Change of the work function of a Mo(110) surface versus Pd doses (min) a) RT deposition, b), c) RT deposition and annealed after each dose at 800 K and 1000 K, respectively.
- Fig. 5 Change of Pd Auger amplitudes and S-peak heights as a function of Pd doses, deposition temperature: 700 K.
- Fig. 6 LEED patterns from Pd on Mo(110) annealed at 700 K, 60 eV, Pd coverages are approximately a) 1 ML, b) 3 ML, c) 12 ML.

- Fig. 7 Change of the work function $\Delta\phi$ and of the Pd and Mo Auger amplitudes of a 12 ML thick Pd layer as a function of annealing temperature. 2 min anneals.
- Fig. 8 a) XPS spectra of Pd 3d core levels before and after 1000 K annealing, initial thickness 12 ML. b) XPS spectra of Pd valence band before and after annealing at 1000 K, RT deposition, 12 ML initial thickness.
- Fig. 9 LEED patterns from Pd deposits on Mo(110), a) $\theta = 12$ ML, annealed at 1150 K, 60 eV. b) - e) $\theta = 5$ ML, annealed at 480 K (b), 815 K (c), 1040 K (d), 1165 K (e), 85 eV.
- Fig. 10 Pd and Mo Auger amplitudes and S-peak heights as a function of annealing temperature, $\theta = 1.06$ ML.
- Fig. 11 Work function change and Pd and Mo Auger amplitudes as a function of annealing temperature, initial Pd thickness 3.5 ML.
- Fig. 12 Work function change, Pd and Mo Auger amplitudes as a function of annealing temperature, initial Pd thickness 5 ML.
- Fig. 13 Reciprocal lattice unit meshes a) of the "complex LEED pattern", b) of (3x1) pattern (solid lines). Dashed lines: Mo unit mesh.
- Fig. 14 Models for Pd-Mo alloy layer structures a) thick layer (12 ML), b) intermediate thickness.

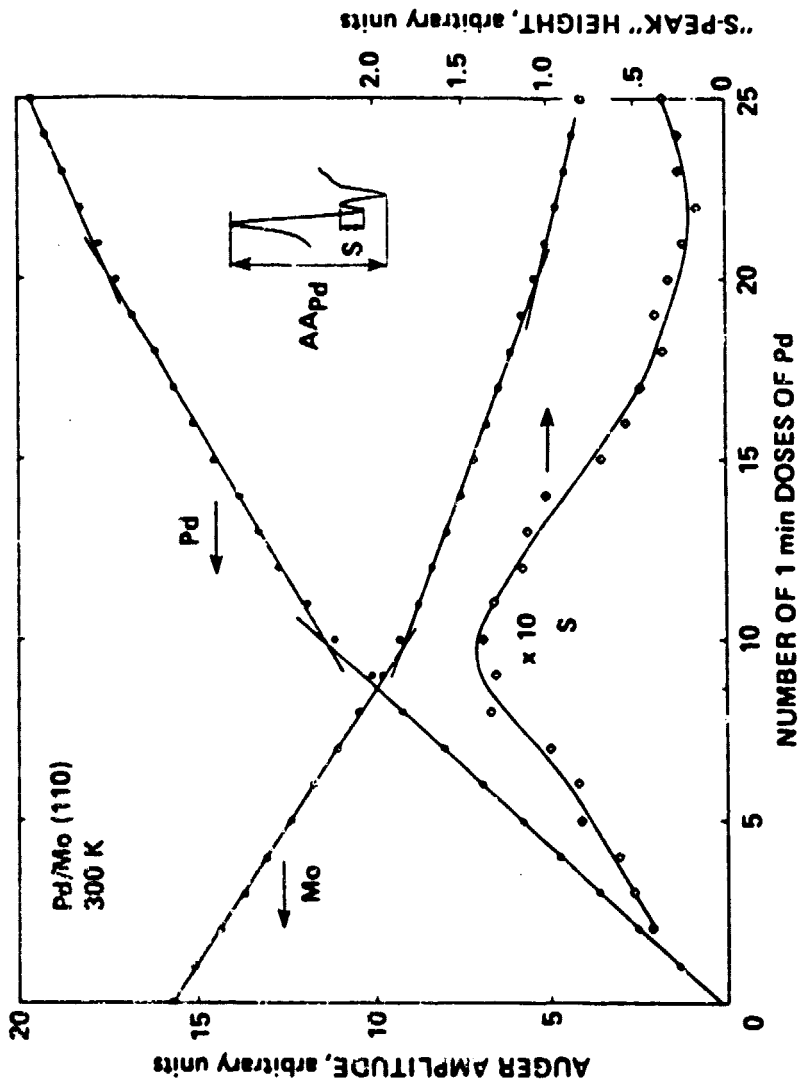
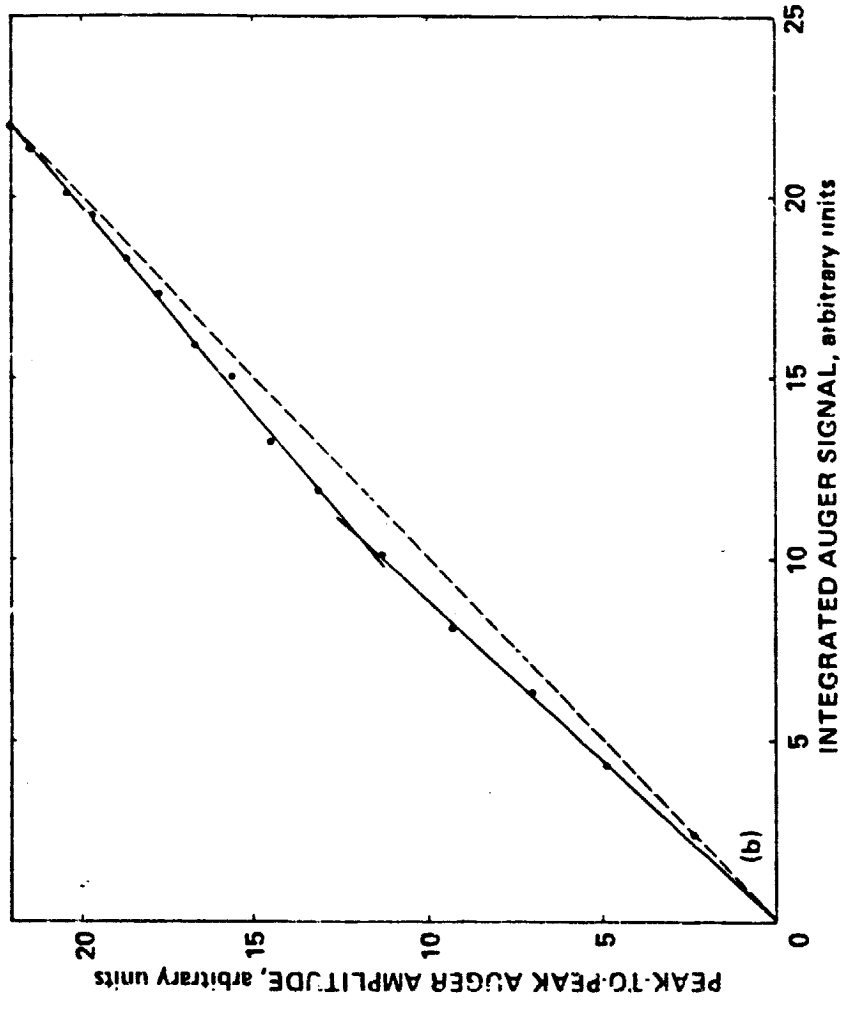


Fig. 10



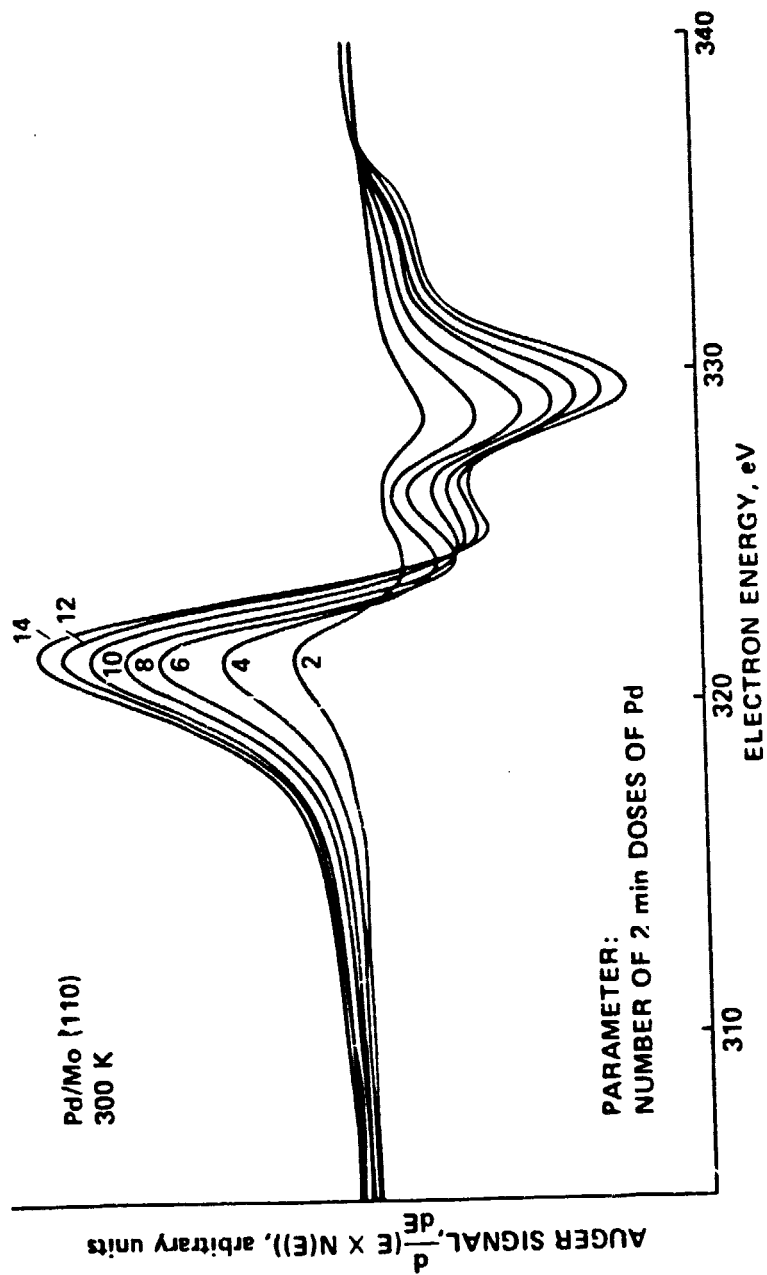
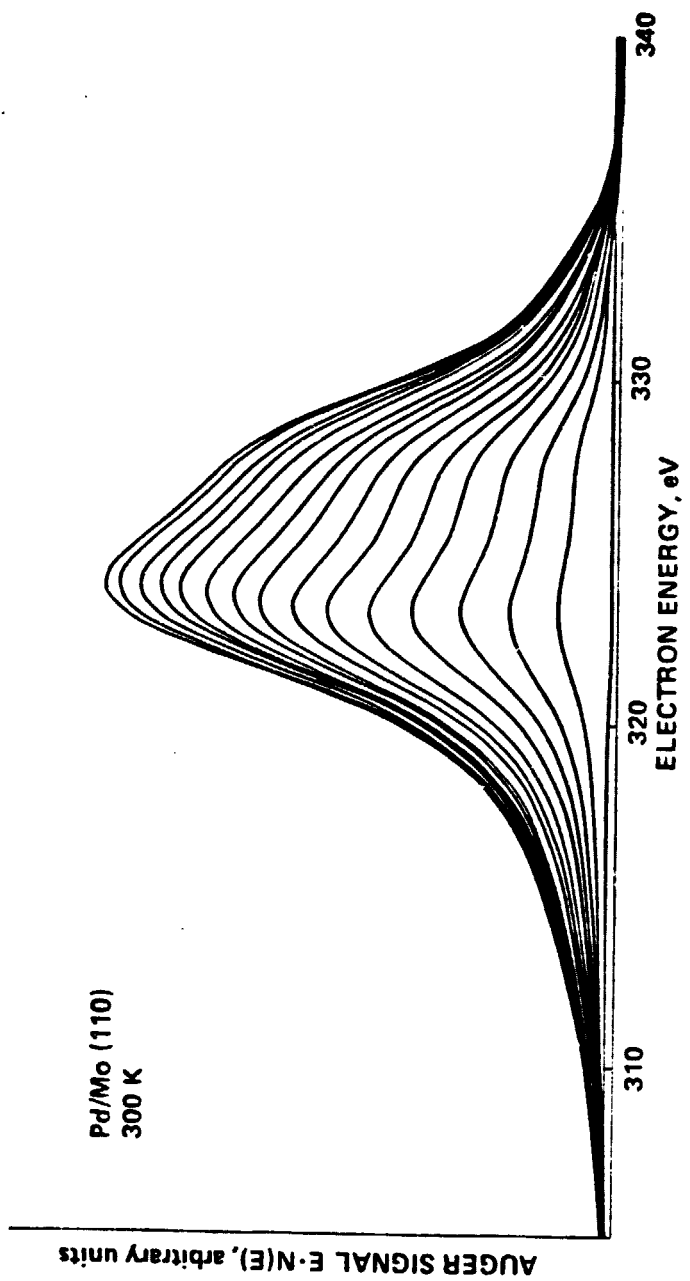


Fig. 2a



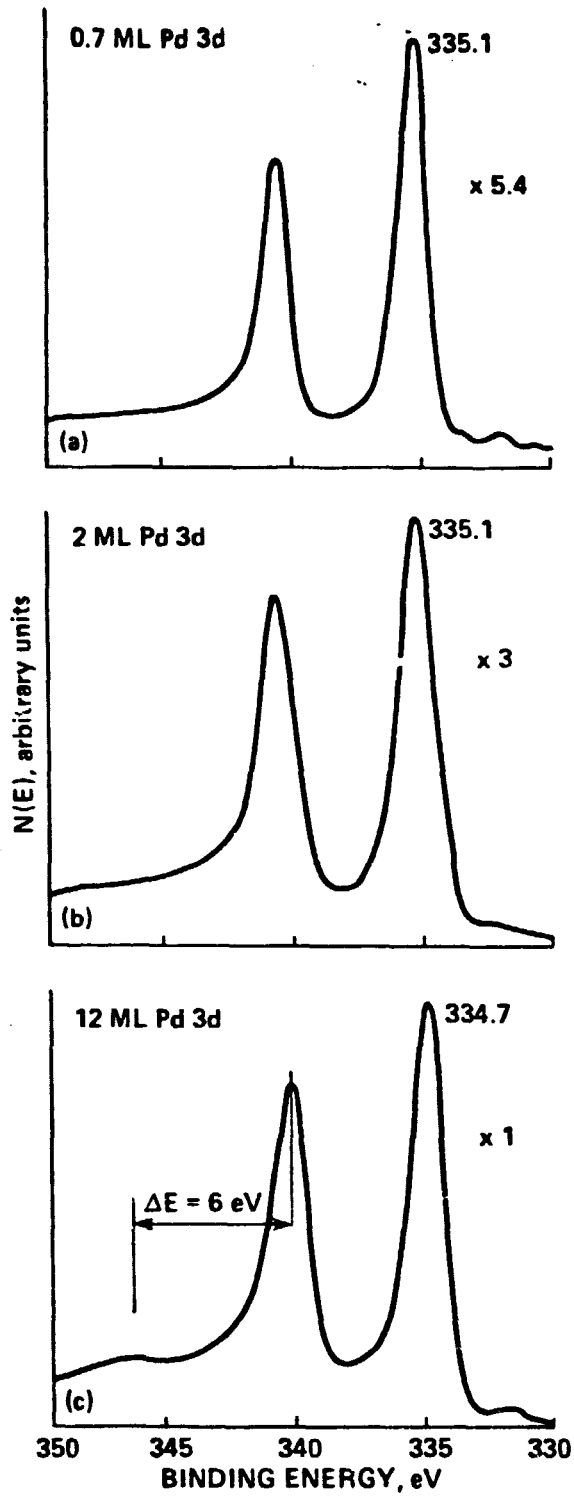
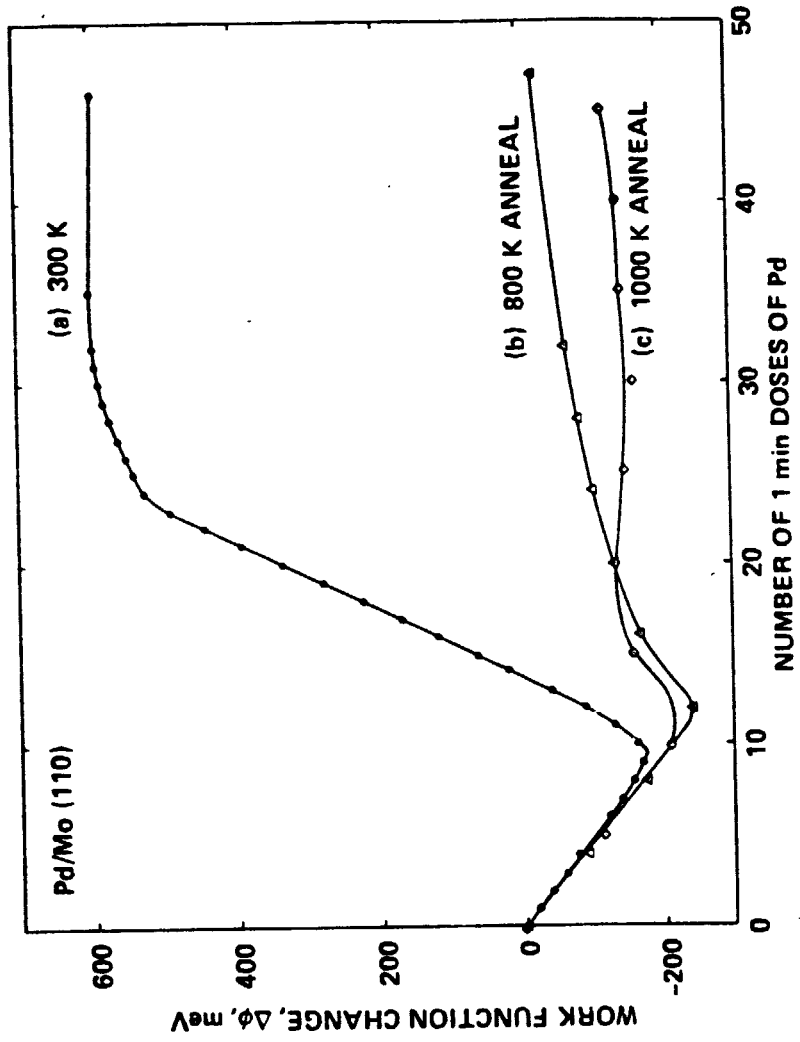


Fig. 3



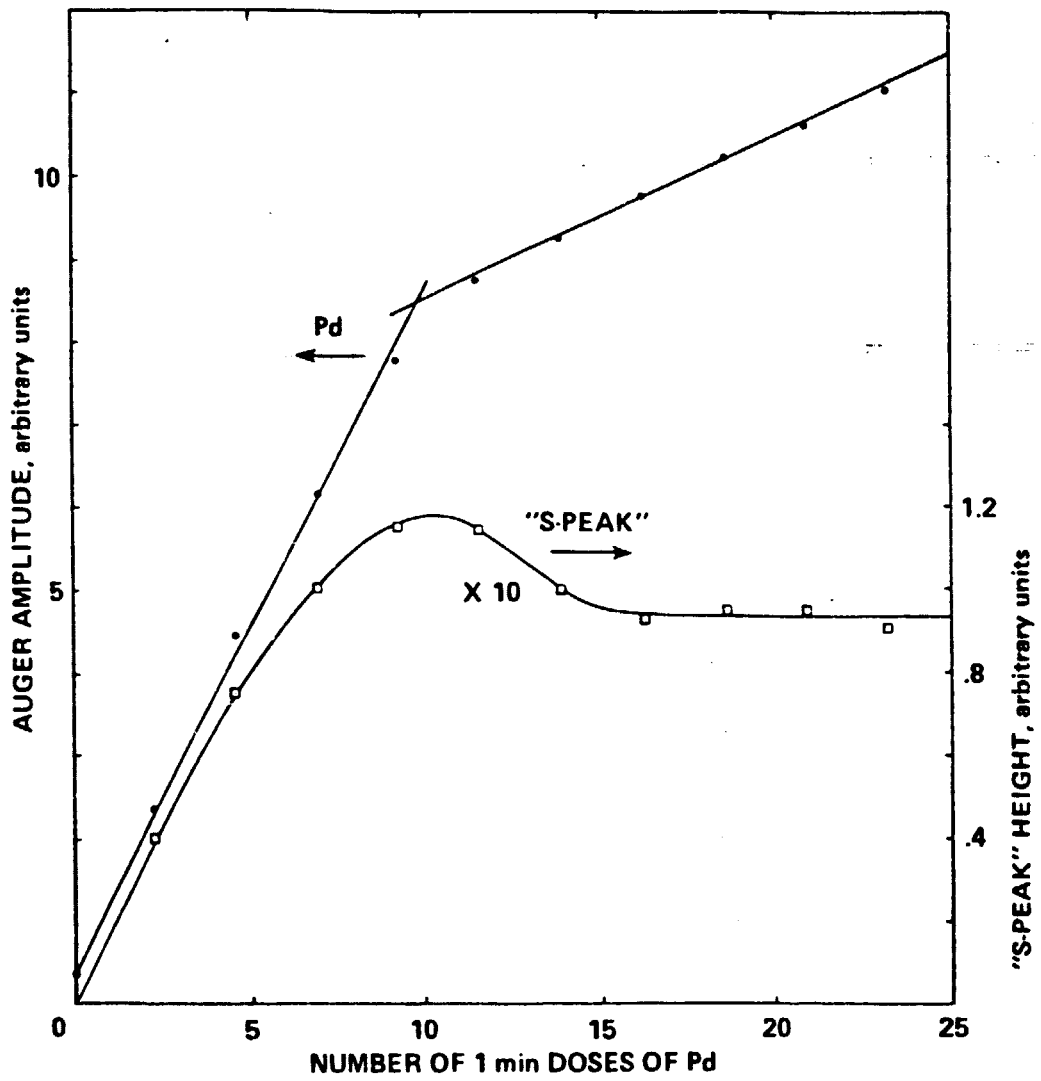
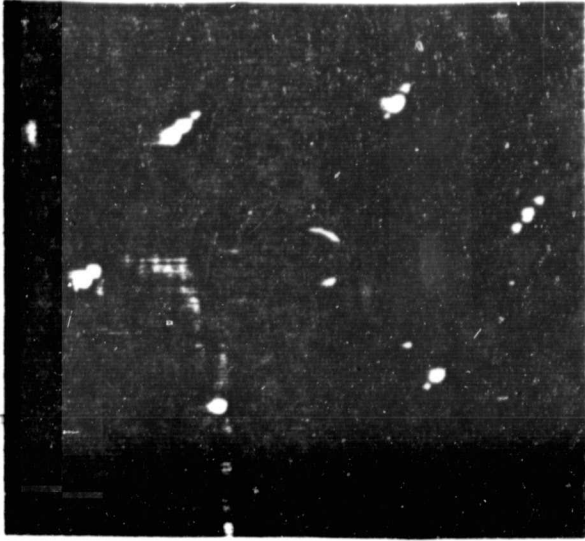
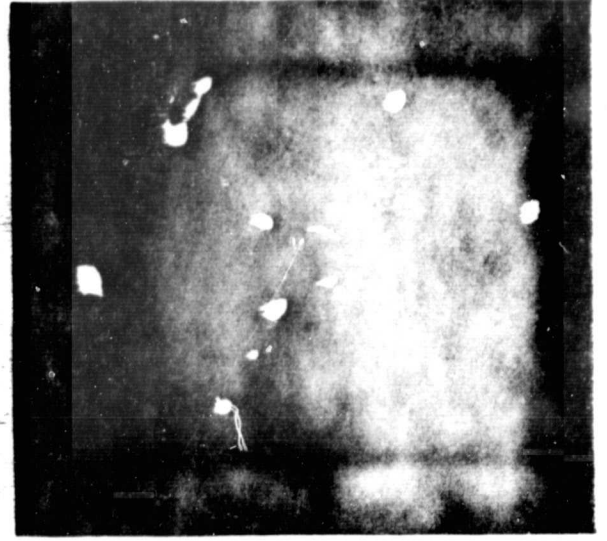


Fig. 5

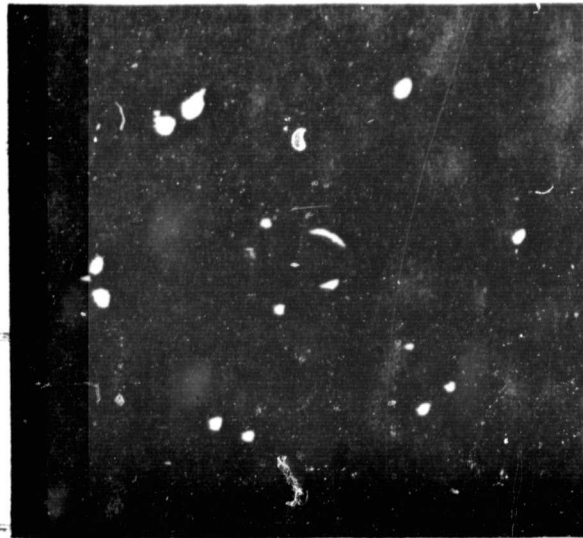
ORIGINAL PAGE IS
OF POOR QUALITY



a



b



c

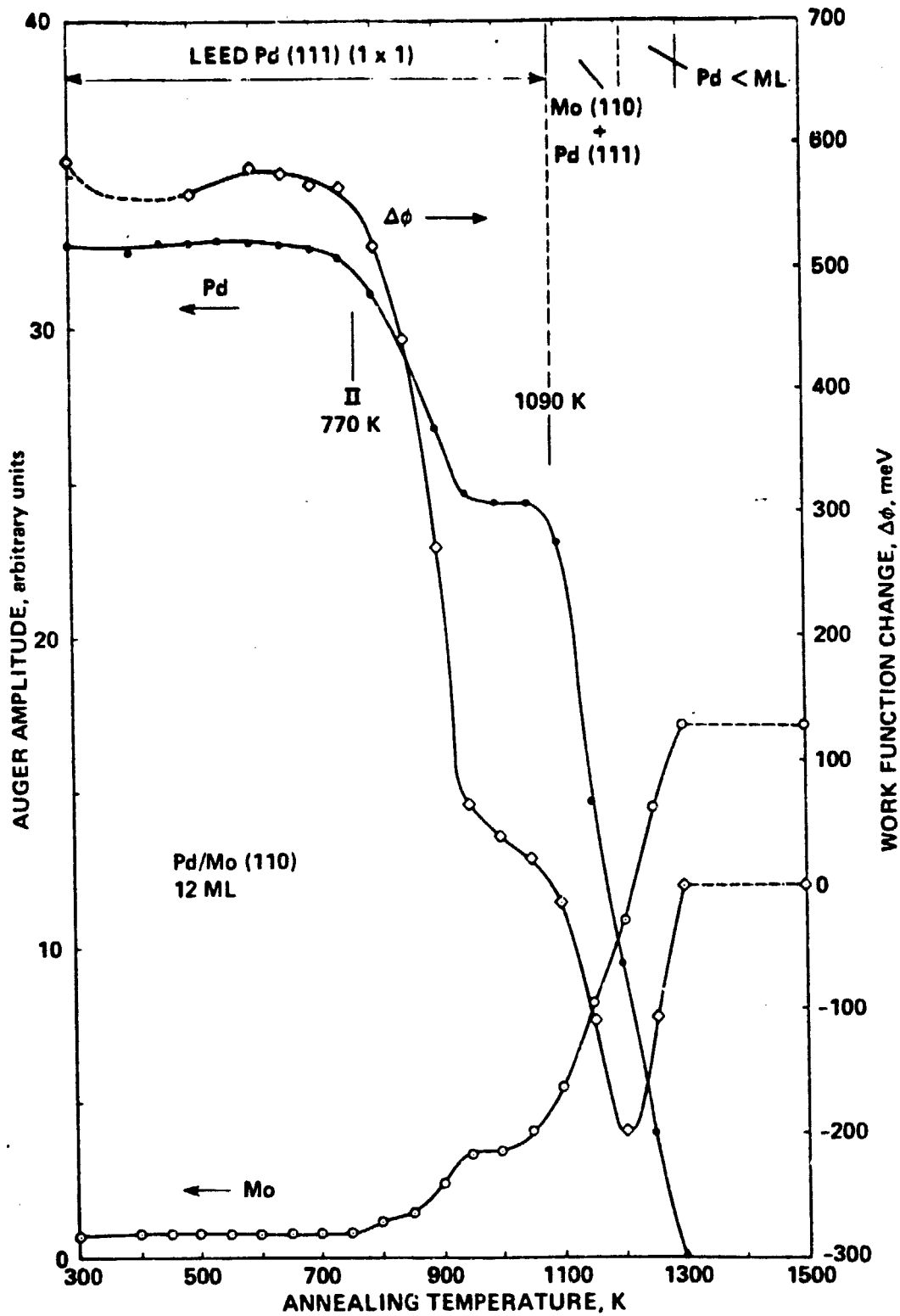


Fig. 7

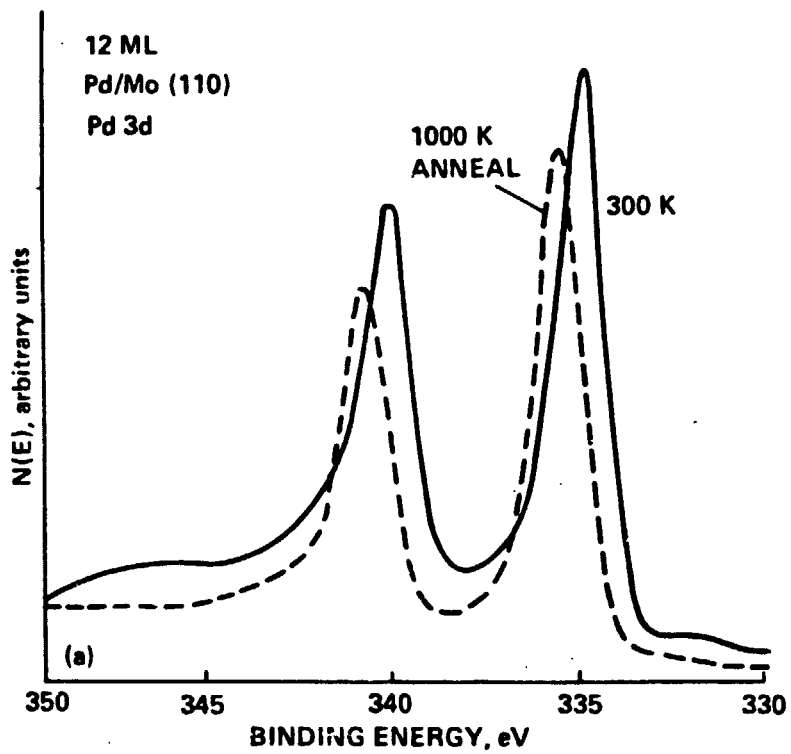


Fig. 8a

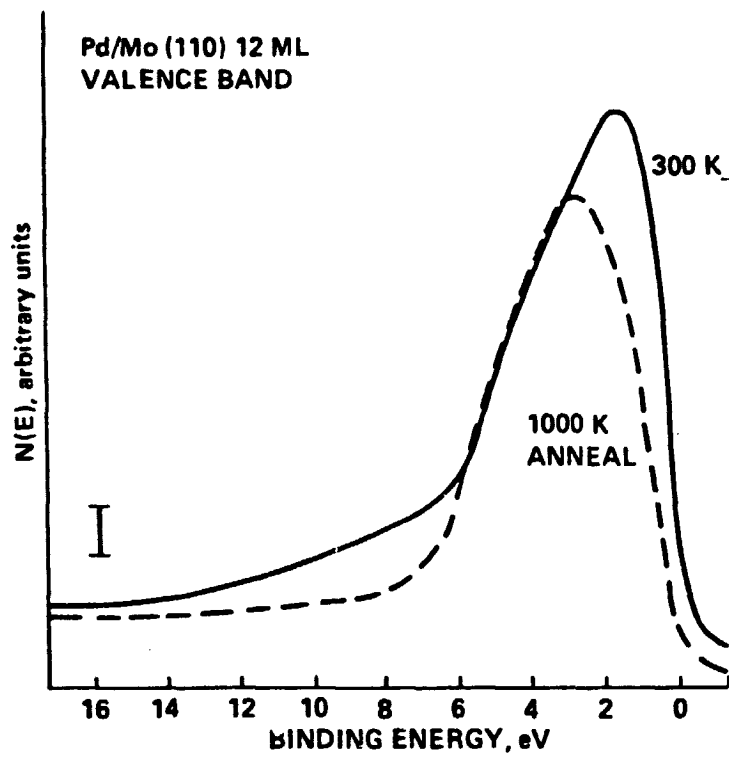
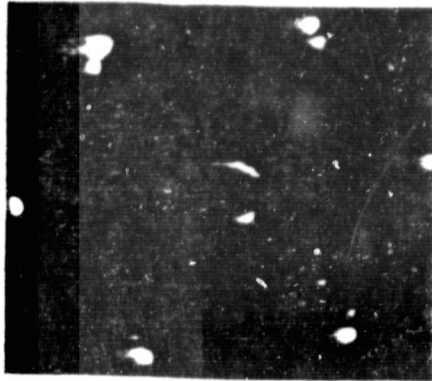
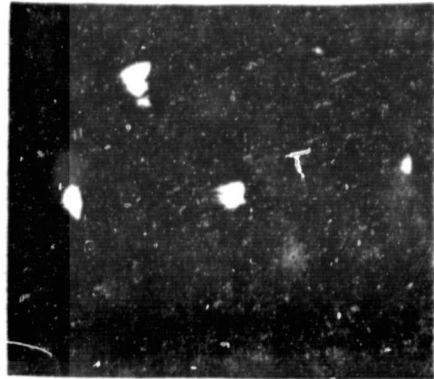


Fig. 8b

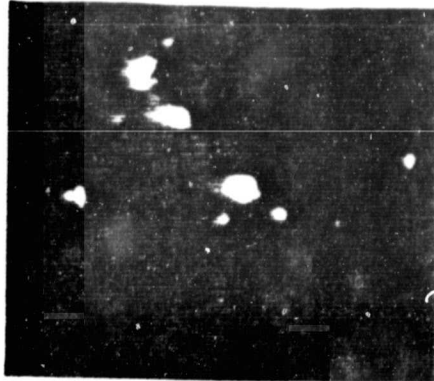
ORIGINAL PAGE IS
OF POOR QUALITY



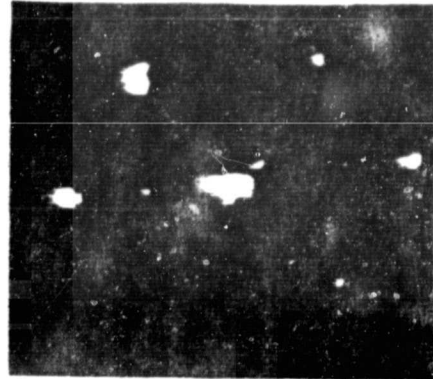
a



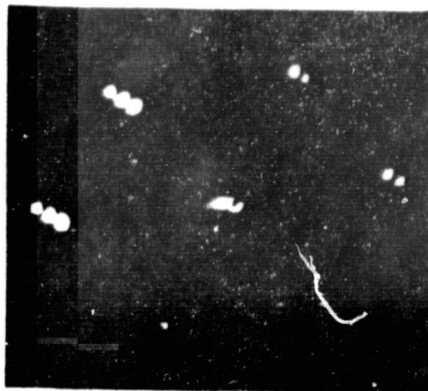
b



c



d



e

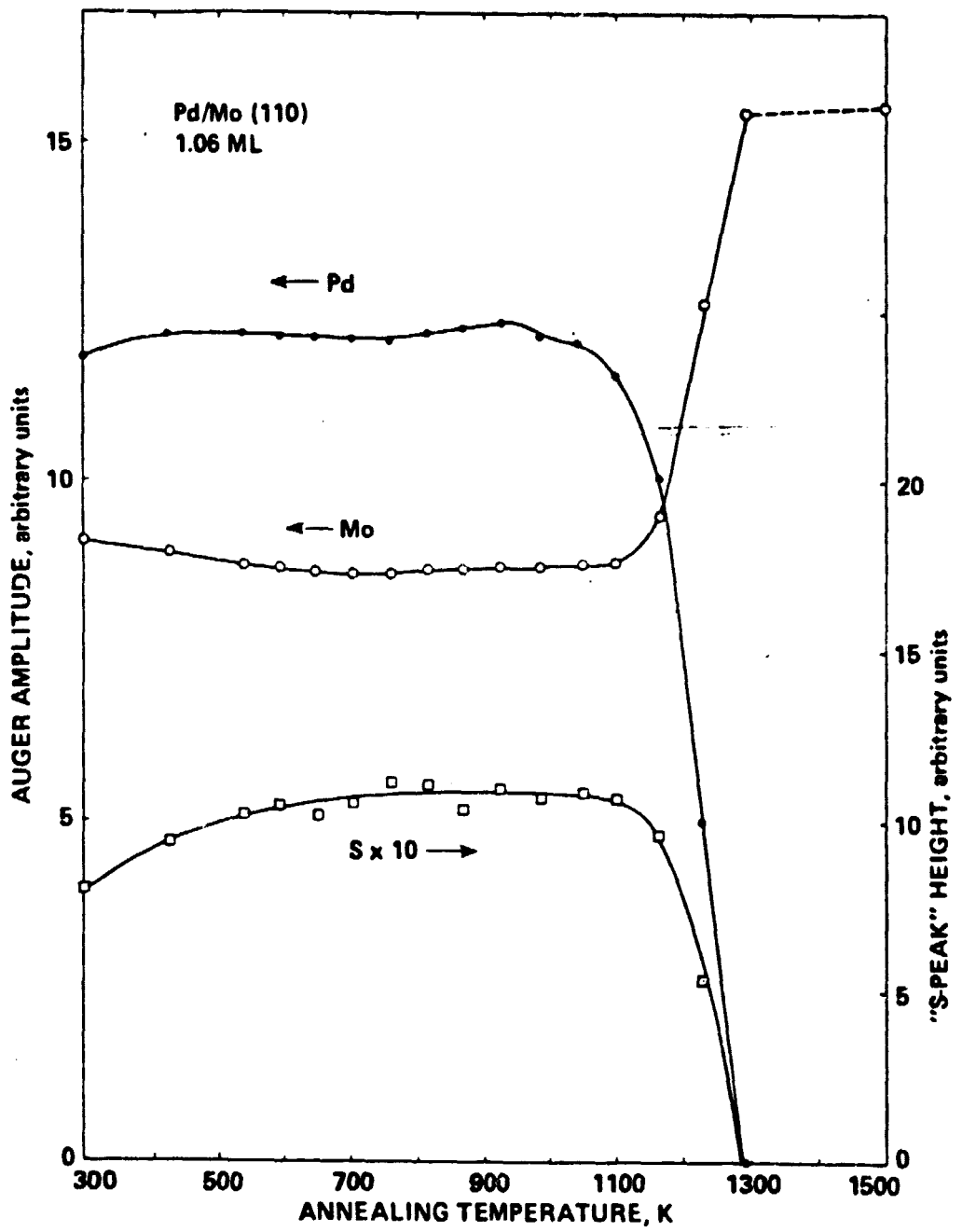


Fig. 10

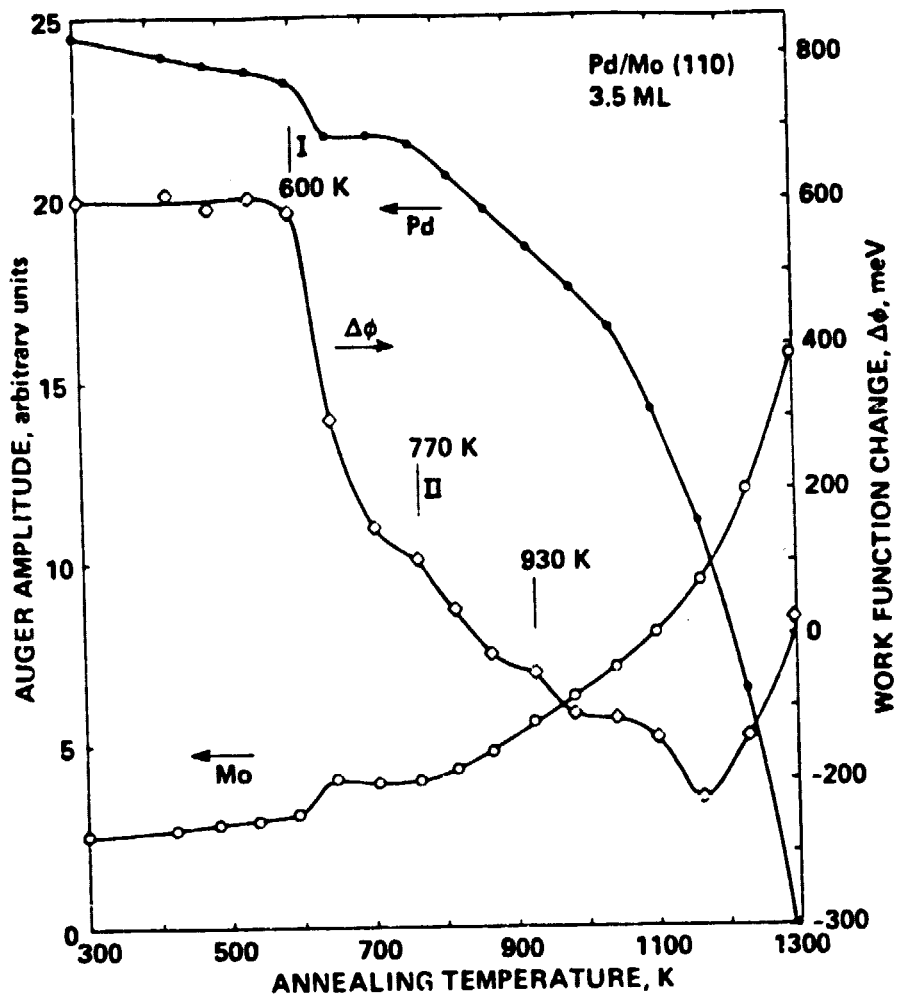


Fig. 11

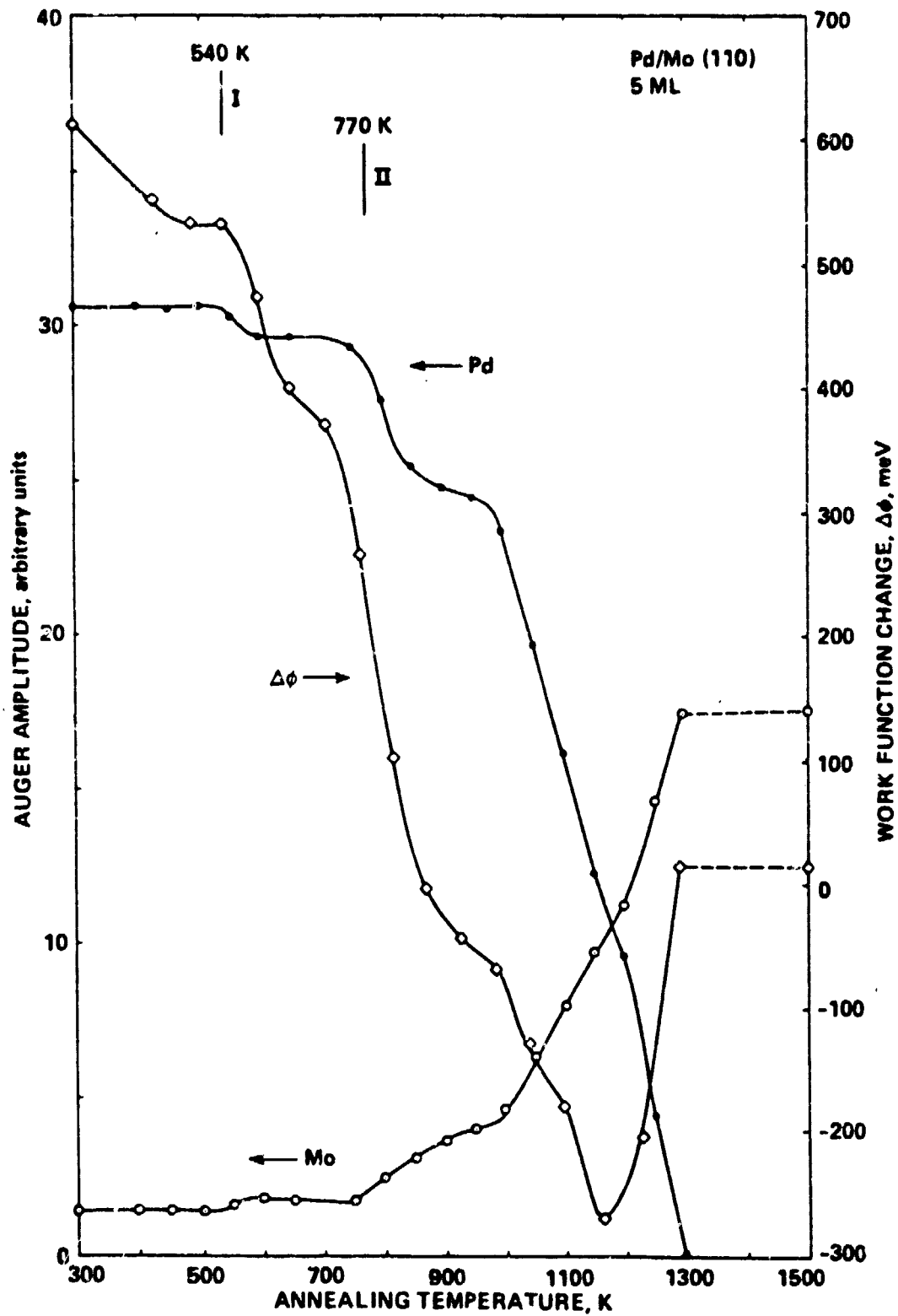


Fig. 12

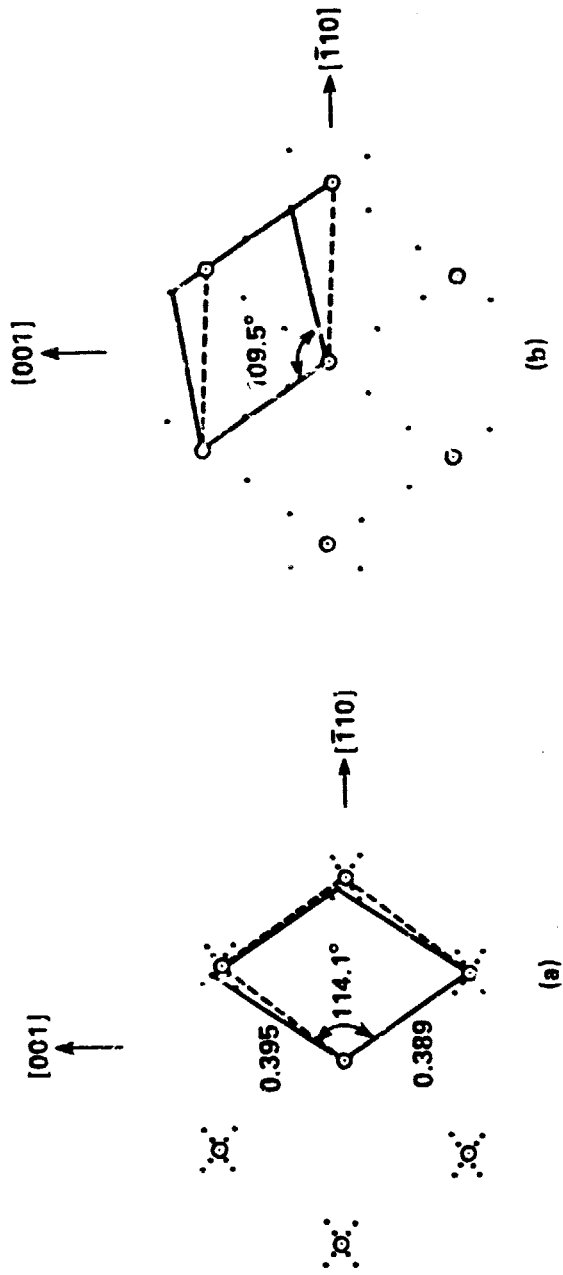
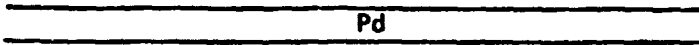
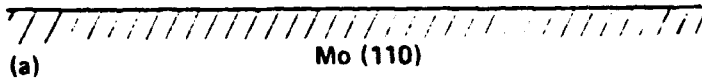


Fig 13



$Pd_y Mo$

$y = 2$ AT 1000 K ANNEAL



BEST "(3 x 1)" WHERE $x = 2$

Pd "(III)" STRUCTURE

